Unfolding is the driving force for mitochondrial import and degradation of Parkinson's disease-related protein DJ-1

Bruno Barros Queliconi[1¶], Waka Kojima[1¶], Mayumi Kimura[1, 2], Kenichiro Imai[3], Chisato Udagawa[1], Chie Motono[3, 4], Takatsugu Hirokawa[3, 5, 6], Shinya Tashiro[7], Jose M.M. Caaveiro[8], Kouhei Tsumoto[9], Koji Yamano[1], Keiji Tanaka[2], and Noriyuki Matsuda[1,*]

[1]Ubiquitin Project, Tokyo Metropolitan Institute of Medical Science, 2-1-6 Kamikitazawa, Setagaya, Tokyo 156-8506, Japan,
[2]Laboratory of Protein Metabolism, Tokyo Metropolitan Institute of Medical Science, 2-1-6 Kamikitazawa, Setagaya, Tokyo 156-8506, Japan,
[3]Cellular and Molecular Biotechnology Research Institute, National Institute of Advanced Industrial Science and Technology (AIST), Tokyo, Japan, 2-4-7 Aomi, Koto-ku, Tokyo 135-0064, Japan,
[4]Computational Bio Big-Data Open Innovation Laboratory (CBBD-OIL), AIST, Waseda University, 3-4-1 Okubo, Shinjuku-ku, Tokyo 169-8555, Japan,
[5]Division of Biomedical Science, Faculty of Medicine, University of Tsukuba, 1-1-1 Tennodai, Tsukuba, Ibaraki 305-8575, Japan,
[6]Transborder Medical Research Center, University of Tsukuba, 1-1-1 Tennodai, Tsukuba, Ibaraki 305-8575, Japan,
[7]Department of Material and Biological Chemistry, Faculty of Science, Yamagata University, Yamagata 990-8560, Japan,
[8]Laboratory of Global Healthcare, Graduate School of Pharmaceutical Sciences, Kyushu University, Maidashi 3-1-1, Higashi-ku, Fukuoka 812-8582, Japan,
[9]Department of Bioengineering, Graduate School of Engineering, The University of Tokyo, 7-3-1 Hongo, Bunkyo-ku, Tokyo 113-8656, Japan.

*Corresponding author: Noriyuki Matsuda (matsuda-nr@igakuken.or.jp)

¶ : These authors contributed equally to this work

Key words: mitochondria, import, Parkinson's disease, DJ-1

Summary Statement

Several mutations in Parkinson's disease-related protein DJ-1 cause its mitochondrial import and degradation. We revealed that protein unfolding is the driving force for the import and degradation of DJ-1.

Abstract

Diverse genes associated with familial Parkinson's disease (familial Parkinsonism) have been implicated in mitochondrial quality control. One such gene, *PARK7* encodes the protein DJ-1, pathogenic mutations of which trigger its translocation from the cytosol to the mitochondrial matrix. The translocation of steady-state cytosolic proteins like DJ-1 to the mitochondrial matrix by missense mutations is rare and the underlying mechanism remains to be elucidated. Here, we show that the protein unfolding associated with various DJ-1 mutations drives its import into the mitochondrial matrix. Increasing the structural stability of these DJ-1 mutants restores cytosolic localization. Mechanistically, we show that a reduction in the structural stability of DJ-1 exposes a cryptic N-terminal mitochondrial targeting signal (MTS) including Leu10 that promotes DJ-1 import into the mitochondrial matrix for subsequent degradation. Our work describes a novel cellular mechanism for targeting a destabilized cytosolic protein to the mitochondria for degradation.

Introduction

A close relationship between neurodegenerative disease and impaired mitochondrial function has been widely recognized. Parkinson's disease is the best-elucidated example with several genes associated with familial early-onset Parkinsonism implicated in mitochondrial quality control. One of those genes, *PARK7*, encodes the cytosolic protein DJ-1. DJ-1 is a relatively small (189 amino acids; <20 kDa) multifunctional protein. The DJ-1/*PARK7* gene was first identified as an oncogene

(Nagakubo et al., 1997), but was later re-identified as causal for recessive familial Parkinsonism, *PARK7* (Bonifati et al., 2003). Countless studies focused on elucidating DJ-1 functionality have since accentuated the pleiotropic nature of the protein. Although conclusions from the myriad studies vary and frequently contradict one another, links between mitochondrial integrity and DJ-1 have been frequently observed.

DJ-1 mitochondrial localization, however, is controversial as wild type and mutant DJ-1 have been reported to localize to either the cytosol or the nucleus (Bjorkblom et al., 2014; Blackinton et al., 2009; Cali et al., 2015; Canet-Aviles et al., 2004; Nural et al., 2009; Ren et al., 2012; Xu et al., 2005; Zhang et al., 2005). Consistent with an initial report (Maita et al., 2013), an earlier study by our group found that wild type DJ-1 is cytosolic under steady state conditions and that pathogenic mutations in the protein trigger translocation to the mitochondrial matrix by an unknown pathway (Kojima et al., 2016). In general, missense mutations in cytosolic proteins rarely result in translocation to the mitochondria. We thus wanted to disentangle the molecular mechanisms underlying the mitochondrial localization of DJ-1 mutants, and then determine the physiological significance of the import.

Here, we show that mitochondria-localized mutants of DJ-1 are prone to unfolding. We found that a reduction in DJ-1 structural stability promotes import into the mitochondrial matrix and subsequent degradation. Furthermore, enhancing the structural stability of DJ-1 can recover the cytosolic localization, implying that protein unfolding is the motive force for DJ-1 mitochondrial import. We thus propose a new mechanism by which destabilized cytosolic proteins (e.g. DJ-1) can be targeted to mitochondria.

Results

Screening for novel DJ-1 mutations that promote mitochondrial localization

Several researchers, including our group, independently reported that some pathogenic DJ-1 mutants (M26I, E163K, and L166P) localize to the mitochondria (Bonifati et al., 2003; Kojima et al., 2016; Maita et al., 2013). Furthermore, proteinase K protection assays of mitochondria isolated from cells expressing the DJ-1 mutants confirmed that the DJ-1 E163K and L166P mutants localize in the mitochondrial matrix despite the absence of a predictable mitochondria/matrix targeting signal (MTS) (Kojima et al., 2016). We thus sought to elucidate the molecular mechanism underlying the mitochondrial import of DJ-1.

First, to identify the region important for cytosolic localization of DJ-1, we performed an Ala scan of the protein and examined the resulting subcellular localization in *DJ-1* knockout HeLa cells (Kojima et al., 2016). Substitution of multiple sites (E16, V23, D24, R28, R48, C53, K63, N76, K89, K93, R98, T124, T125, H126, L128, and R156) had no effect on the cytosolic localization of DJ-1. In contrast, Ala replacement of E15, E18, R27, V33, T34, D68, or I105 resulted in mitochondrial translocation (Fig. 1A, and Figs. S1A and S1B). The mutation sites of these new Mitochondria-Localized DJ-1 Mutants (hereafter referred to as MLMs) are dispersed throughout the DJ-1 sequence, strongly suggesting that there is no “hotspot” or restricted area in the DJ-1 structure that promotes mitochondrial localization. Using ASA View (Ahmad et al., 2004) to examine the correlation between the subcellular localization of each mutant and the solvent accessibility of the mutated amino acid position, we found that a majority of the MLM sites are buried in the DJ-1 structure (Figs. 1B and 1C), indicating that mitochondrial localization is correlated with DJ-1 instability. Consequently, we extended mutational analyses of the DJ-1 sequence to include various missense mutations that introduced amino acids with bulkier sidechains than Ala into the buried region. Although the initial Ala scan of some residues (E16A, V23A, T124A, and T125A) in the solvent inaccessible regions did not result in mitochondrial translocation (Fig. S1A), subsequent

substitution with bulkier or less compatible amino acids (E16W, V23R, T124R, and T125R) generated the mitochondria-localized phenotype (Fig. 1A, and Fig. S1A). Substitution with bulkier amino acids at A14, V44, A104, and C106 also caused the mitochondria localization (Fig. 1A). For quantitative co-localization and statistical analysis, the co-localization of various DJ-1 mutants with TOMM20 (mitochondrial marker) in individual cells were calculated as a Pearson correlation coefficient. The Pearson correlation coefficients for 21 cytoplasmic mutants were between 0 and 0.25 (Fig. 1D). Conversely, these values for the 22 mitochondrial mutants were much higher and ranged from 0.6-0.9 (Fig. 1E). A number of mutants (I21T, S47A, H126A, and P127A), however, had more varied values (0.1-0.6), suggesting they show variable or mixed localization (Fig. 1D, and Fig. S1C). These quantitative analyses (Figs. 1D and 1E) are consistent with the immunocytochemical findings (Fig. 1A, and Fig. S1). In total, ~ 93% of mutations in the DJ-1 buried structure (ASA value < 0.1) caused mitochondrial localization, whereas ~ 85% of the mutations in the non-buried structure (ASA value > 0.1) remained cytosolic (Fig. 1C). Therefore, we surmised that structural disturbances rather than disruption of specific regions of DJ-1 were the basis for the unique mitochondrial localization. Only one mutation (L10P) in the DJ-1 buried structure (ASA value = 0) remained cytosolic (Fig. 1C, arrowhead) and is studied in detail later in this paper.

Stability of mitochondria-localized pathogenic DJ-1 mutants

Next, we sought to investigate the stability of purified DJ-1 mutant proteins. We first focused on the pathogenic DJ-1 mutants. N-terminal 6xHis-tagged DJ-1 proteins with defined pathogenic mutations were purified and their folding stability was measured using thermal shift assays (Lo et al., 2004; Semisotnov et al., 1991). In this assay, recombinant DJ-1 is incubated with thermofluor, and the stability curve is obtained by gradually increasing the temperature and measuring the fluorescence. When DJ-1 unfolds, the exposed hydrophobic surfaces bind the thermofluor, resulting

in an increase in fluorescence. Unfolding temperatures, which are analogous to melting temperatures (referred to as Tm), indicate the maximum value of the first derivative of the relative fluorescence unit (RFU) as a function of temperature (dRFU/dT) (Figs. 2A and 2B). Cytosolic pathogenic mutants had Tms that exceeded 63.5°C, whereas Tms for the mitochondrial localized mutants were significantly lower than wild-type Tm and had a maximum Tm of 60.5°C. Two pathogenic mutants, L10P and L166P, had no detectable Tm suggesting they are unable to initiate protein folding properly (Olzmann et al., 2004; Prahlad et al., 2014; Ramsey and Giasson, 2010). To further confirm destabilization of the DJ-1 mutants, we measured the sensitivity of each mutant to trypsin digestion under more physiological temperatures (normal body temperature 37°C). The pathogenic MLMs M26I, E163K, and L166P were more susceptible to complete digestion than WT, suggesting their structures are less ordered. Conversely, trypsin digestion of the cytosol-localized mutants E64D and N76D was comparable to WT (Figs. 2C and 2D). The thermal shift and trypsin digestion assays thus support differences between in the folding states of cytosol-localized and mitochondria-localized pathogenic DJ-1 mutants. The exception to this conclusion, however, is the cytosolic mutant, L10P (Fig. 1D), which is highly sensitive to trypsin digestion (Fig. 2D) in addition to being thermally unstable (Fig. 2B). Although this mutant initially seems to conflict with our hypothesis that DJ-1 protein destabilization promotes mitochondrial translocation, additional analyses of this mutant (discussed in greater detail later in the paper) highlight the likelihood of a cryptic N-terminal mitochondria targeting sequence.

Since DJ-1 is a causative gene for familial Parkinson's disease, we sought to assess whether the mislocalization of pathogenic DJ-1 mutants stresses mitochondria when expressed over long periods of time. To facilitate these analyses, we used OPA1, PGAM5, and ATF4 as mitochondrial stress indicators (Anand et al., 2014; Quiros et al., 2017; Sekine et al., 2012). When wild-type DJ-1 or mitochondria-localized pathogenic mutants E163K and L166P were expressed in *DJ-1* knock-out cells for 48 hours, no difference was observed in the cleavage pattern of PGAM5 and OPA1, or on

the induction of ATF4 (Fig. S2, lanes 1 - 4). Addition of the mitochondrial uncoupler valinomycin resulted in cleavage of both PGAM5 and Opa1 and induction of ATF4, indicating that the assay system was viable (Fig. S2, lanes 5 - 6). We thus conclude that the mitochondrial localization of the pathogenic DJ-1 mutants does not induce mitochondrial stress relevant to the onset of Parkinson's disease (discussed in greater detail later).

Correlation between DJ-1 mutant instability and mitochondrial localization

If our hypothesis that perturbations in protein folding affect DJ-1 localization is correct, then it should be possible to modulate the subcellular localization by altering the side-chain character of specific amino acids. To test this, we iteratively replaced E18, which resides within a central position in the DJ-1 structure, with other amino acids and assessed the effects on both protein stability and subcellular localization. Although localization of the E18D, E18N, and E18Q mutants has been previously reported as cytosolic (E18D) or mitochondrial (E18N and E18Q) (Blackinton et al., 2009), we generated all E18X mutants and assessed their localization when expressed in *DJ-1* knockout HeLa cells. Overall, we found that the E18X mutants had three distinct localization patterns: exclusively cytosolic, exclusively mitochondrial, or a combination of both phenotypes (Fig 3A). Because some mutants exhibited mixed localization, we tried to quantify the degree of localization for all E18X mutants. We calculated the Pearson correlation coefficient between the DJ-1 E18X mutants and TOMM20 for individual cells (Fig 3B). The positive control, co-localization of Su9-GFP with TOMM20, yielded a value of 0.8 (Fig 3B column 1), whereas the negative control, co-localization of cytosolic GFP with TOMM20, was ~ -0.2 (Fig 3B column 2). The coefficients for the mutants (E18T, E18D, E18S, and E18C) that exhibited cytoplasmic localization comparable to WT were 0 to 0.3. Mutants with mixed cytoplasmic and mitochondrial localization (E18T, E18D, E18S, and E18C) had coefficients of 0.5 to 0.7. In contrast, the values for the ten mutants (E18H, E18N, E18V, E18Y, E18R, E18F, E18I, E18P, E18W, and E18K) that

exclusively localized to mitochondria were 0.75 to 0.8, which was equivalent to the positive control (Su9-GFP). These data are consistent with the immunocytochemical findings (Figs. 3A, 3B). To examine the relationship between mitochondrial localization and DJ-1 destabilization, we purified recombinant proteins for all of the E18 mutants with C-terminal 6xHis-tag and examined their susceptibility to trypsin digestion. A clear correlation between trypsin sensitivity and mitochondrial localization was observed (Fig. S3A). For more precise quantification, we also measured the Tms of the E18X mutants (Fig. 3C and Fig. S3B). Although thermal spectra for most of the E18X mutants were characterized by a single peak (e.g. E18T spectrum in Fig. S3B), those of the E18A, E18L, and E18N mutants had two peaks, suggestive of bimodal unfolding transitions (Fig. S4). The Tms for these mutants were: E18A - 57.5°C and 61.2°C; E18L - 55.8°C and 61.8°C; and E18N - 58.5°C and 63°C. We speculate that the higher Tm transitions are due to oxidation of C106 given the reported presence of oxidized Cys106-SO_2^- in the E18A and E18N DJ-1 mutants (Prahlad et al., 2014). The E18K and E18R mutants had no detectable unfolding transition, suggesting they are largely unstructured. We found that the E18X mutants that localize to the cytosol (E18S, E18T, E18C, and E18D) had Tms of more than 60°C, whereas a majority of the exclusively mitochondria-localized mutants (E18H, E18F, E18Y, E18I, E18W, E18P, E18K, and E18R) had substantially reduced thermal stabilities (>11°C) compared to WT (Fig. 3C). These data clearly indicate that DJ-1 instability directly correlates with the mitochondrial localization state.

Destabilized DJ-1 mutant localizes inside the mitochondrial matrix

The dataset presented so far does not rule out the trivial possibility that the DJ-1 mutants are attached to the mitochondrial surface rather than being translocated to the mitochondrial matrix. We thus sought to confirm matrix localization of the HA-tagged DJ-1 mutants. First, we assessed the utility of different permeabilization methods for immunocytochemical analysis. Triton X-100 (1%) permeabilizes both the outer mitochondrial membrane (OMM) and inner mitochondrial membrane

(IMM) and enables antibodies to access matrix proteins such as mitochondrial Hsp60, whereas digitonin (50 μg/mL) does not sufficiently permeabilize the IMM (Kojima et al., 2016; Okatsu et al., 2015a) for Hsp60 detection (Fig. 4A). For the E18K mutant, anti-HA immunoreactivity was not observed in the mitochondria after permeabilization with digitonin but was detectable following Triton X-100 permeabilization (Fig. 4B). Since DJ-1 E18K mutant was exogenously transfected into cells, it is possible that the DJ-1(E18K) was not fully introduced in the digitonin-permeabilized cells. To address this concern, cells were transfected with a GFP-IRES-DJ-1(E18K) plasmid and then subjected to immunocytochemistry. GFP-IRES-DJ-1(E18K) guarantees the expression of the E18K mutant in GFP-expressing cells. In the GFP-positive cells, the E18K mutant-derived signal remained undetectable following digitonin permeabilization but, as before, was present with Triton X-100 permeabilization (Fig. 4C). These results confirmed mitochondrial matrix localization of the mutant.

The dependence of DJ-1 translocation on the mitochondrial membrane potential (ΔΨm) also supports mitochondrial matrix localization. The ΔΨm is generated across the IMM and is essential for canonical matrix-localized proteins to pass the IMM (Hartl et al., 1989). Treatment of cells with uncouplers such as valinomycin and carbonyl cyanide *m*-chlorophenyl hydrazine (CCCP) dissipate the ΔΨm. Pre-treating cells with either of the two uncouplers prior to transfecting the DJ-1 E18K mutant resulted in cytosolic localization rather than the mitochondrial localization typical of the mutant (Fig. 4D). These results indicate that the DJ-1 E18K mutant is imported into the matrix in a ΔΨm-dependent manner.

Mitochondrial translocases facilitate localization of DJ-1 mutants to the IMM

Mitochondrial matrix protein precursors are imported into the matrix by sequential passage through TOMM40 (core channel component of translocases on the outer membrane complex; TOMM complex) and TIMM23 (core channel component of the inner membrane complex; TIMM23

complex). Since TOMM40 and TIMM23 are essential genes, functional analysis of their role in DJ-1 E18K mitochondrial localization could not be performed using knock-out cell lines. Instead, we utilized Small interfering RNA (siRNA)-mediated knockdown to suppress expression of the endogenous TOMM40 and TIMM23 proteins (Fig. 5A). As a model precursor protein for targeted matrix import, we used Su9-GFP, which utilizes the amino-terminal region of FoATPase subunit 9 (Su9) to direct GFP to the matrix via the TOMM and TIMM23 complexes (Ishihara et al., 2006). Knockdown of either TOMM40 or TIMM23 by siRNA reduced the mitochondrial localization of Su9-GFP (Fig. 5B). Quantification of the degree of co-localization between Su9-GFP and TOMM20 confirmed that the mitochondrial translocation of Su9-GFP was reduced following knockdown of TOMM40 and TIMM23 (Fig. 5D). A decrease in the mature (processed) form of Su9-GFP was also observed (Fig. 5A). These results confirmed that knockdown of TOMM40 and TIMM23 impedes protein import into the matrix. For WT DJ-1, cytosolic localization was not affected in either the immunocytochemical or quantification-based analyses following knockdown of TOMM40 or TIMM23 (Fig. 5C and 5E). Conversely, mitochondrial localization of the E18K mutant was clearly inhibited following knockdown of TOMM40 or TIMM23 in the immunocytochemical images (Fig. 5F), and these results were further substantiated by quantitative analysis (Fig. 5H). Mitochondrial localization of the E18H mutant was likewise inhibited (Fig. 5G and 5I). The immunocytochemical data shown in Figs. 4 and 5, in conjunction with previous reports describing matrix localization of DJ-1 E18A/H126A mutants (Kojima et al., 2016; Maita et al., 2013), indicate that matrix localization of DJ-1 mutants depends on TOMM40, TIMM23, and an intact $\Delta\Psi m$.

The amino terminus of DJ-1 functions as a destabilization-dependent MTS

We next tried to identify the region responsible for mitochondrial localization of the DJ-1 MLMs. To narrow down the DJ-1 mitochondrial localization domain, we performed domain-swaps with a

prokaryotic homolog of human DJ-1, the *E. coli* protein YajL (Fig. 6A). YajL and DJ-1 have 38% amino acid sequence identity and their crystal structures have almost identical backbone structures with a Cα root-mean-square deviation (RMSD) value of two angstroms (Wilson et al., 2005). When expressed in *DJ-1* knockout HeLa cells, both WT DJ-1 and YajL are cytosolic (Fig. 6B, top panels). C-terminal deletion of DJ-1 [removal of residues 135-189, abbreviated as DJ-1ΔC] promoted mitochondrial translocation, whereas deletion of the same region of YajL [removal of residues 135-196, abbreviated as YajLΔC] did not affect its cytosolic localization (Fig. 6B, middle panels). We thus assessed the effects of domain-swaps between YajLΔC (cytosolic localization) and DJ-1ΔC (mitochondrial localization) to identify the essential mitochondrial localization region of DJ-1ΔC. An N-terminal DJ-1 and C-terminal YajL (abbreviated as DJ1/YajLΔC) chimera localized to the mitochondria, whereas the reciprocal chimera, N-terminal YajL and C-terminal DJ-1 (abbreviated as YajL/DJ1ΔC), was cytosolic (Fig. 6B, bottom panels). Pearson-based quantitative analysis confirmed the immunocytochemical findings (Fig. 6C). Thus the DJ-1 N-terminal region (residues 1-64), which was sufficient to drive translocation of YajL(64-134) to the mitochondria, functions as a novel type of signal for mitochondrial translocation.

Based on previous structural data (Honbou et al., 2003; Olzmann et al., 2004; Tao and Tong, 2003; Wilson et al., 2003), it is clear that DJ-1 does not possess typical MTS structures that form an amphiphilic α-helical structure with hydrophobic residues on one side and positively charged residues on the opposite side. However, when the PA score (Positively charged Amphiphilicity score) from the novel prediction algorithm MitoFates was considered in our search for a cryptic mitochondria-targeting signal (Fukasawa et al., 2015), two candidate regions corresponding to residues 4-13 (Region A) and residues 25-34 (Region B) were predicted (Fig. 6D). To determine if these regions are responsible for the mitochondrial localization of the DJ-1 mutants, we introduced mutations into both regions of DJ-1(E18K) and examined whether the mutation affected mitochondrial localization. We previously showed that single mutations (R27A, V33A, or T34A) in

Region B (Fig. 1A) in the absence of the E18K mutation promoted mitochondrial localization of DJ-1, suggesting that the WT residues do not comprise the mitochondrial targeting motif. Furthermore, when V33 and T34 were substituted with proline, no change in the mitochondrial localization of the E18K mutant was observed (Fig. 6E, right column). In contrast, when R5, L7, L10, or K12 in Region A were substituted with proline, mitochondrial localization of the E18K mutant was clearly impeded (Fig. 6E, and Fig. 6F), indicating that Region A is responsible for mitochondrial targeting of MLM. This finding also explains the initial discrepancy between protein stability and cytosolic localization of the L10P mutation shown in Figs. 1 and 2, as L10 comprises a portion of the cryptic signal in Region A that is essential for mitochondrial import.

In general, to prove that a sequence is a MTS, we need to show that addition of the sequence to a cytoplasmic marker protein (such as GFP) redirects localization to the mitochondria. For example, the amino-terminal region of subunit 9 of the FoATPase (Su9) targets GFP to the mitochondria (Figs. 5A and 5B). To confirm that the N-terminal region of DJ-1 functions as a MTS, we fused amino acids 1-43 of DJ-1 to GFP and examined its subcellular localization. The fusion (DJ43-GFP), however, did not change the cytosolic localization of GFP (Fig. 6G). This result is consistent with our previous data that showed fusion of GFP to the carboxyl terminus of DJ-1 mutants (E18A, M26I, and L166P) did not promote mitochondrial localization, even though both HA-tagged and non-tagged DJ-1 mutants harboring the same mutations localized to mitochondria (Kojima et al., 2016). Given its destabilization-dependency, we speculated that the nature of the DJ-1 MTS differs from the typical MTS. We thus switched to a less stable marker protein, α-synuclein (SNCA), which unlike the stable GFP structure (Ormo et al., 1996), is naturally unstructured and does not form a specific conformation (Theillet et al., 2016). Indeed, recombinant GFP had a high Tm value (Tm = 79 °C) in our thermal shift analysis, while the Tm for recombinant SNCA could not be defined (Fig. 6H). Under steady-state conditions, SNCA is cytosolic but the addition of DJ-1

residues 1-43 promoted mitochondrial import (Fig. 6G, DJ43-SNCA). Moreover, fusion with a smaller segment of the DJ-1 N-terminus that was largely limited to Region A (residues 1-17) was sufficient for mitochondrial localization of SNCA (Fig. 6G, DJ17-SNCA), whereas the same region had no effect on GFP localization (Fig. 6G, DJ17-GFP). As expected, the thermal shift analysis confirmed that DJ17-GFP was tightly folded (Tm = 79 °C), whereas DJ17-SNCA was unfolded with an undetectable Tm (Fig. 6I). Pearson-based quantitative analysis confirmed that Region A of DJ-1 has stronger mitochondria-localization activity than the larger 43 amino acid sequence (Fig. 6J). Mitochondrial localization of DJ17-SNCA was completely inhibited by CCCP treatment (Fig. 6K), indicating that the DJ-1 N-terminus does not attach SNCA to the surface of mitochondria, but rather transports the protein into the mitochondrial matrix. Taken together, these results demonstrate a functional role for Region A as a conformation-dependent MTS.

Dual degradation systems for destabilized DJ-1

To investigate the fate of mitochondria-localized denatured DJ-1 proteins, we established an experimental system in which IRES (internal ribosome entry site)-connected DJ-1 and GFP (an internal control) were simultaneously and transiently expressed following doxycycline (Dox) induction (Fig. 7A). Using this system, transient expression of DJ-1 mutants was induced for 24 h with Dox treatment in *DJ-1* knockout HeLa cells, which was then removed and differences in the amount of DJ-1 protein were assessed. WT DJ-1 was stable and clearly observed 48 h post-Dox induction (Figs. 7B, 7C, upper two panels). In contrast, the E18K and M26I mutants, which undergo mitochondrial translocation, were not observed at the later time point (Figs. 7B, 7C, lower two panels). After normalizing to the GFP internal control, protein quantification revealed that the level of WT DJ-1 underwent a modest 5% reduction at 24 h post-induction, whereas the M26I mutant decreased 35% and the E18K mutant ~ 87% (Fig. 7D). Immunocytochemical analysis confirmed these results. In cells co-expressing E18K and GFP, a significant percentage (~ 45-55%)

of cells were initially positive for both GFP and mitochondrial DJ-1, however, most of the mitochondrial signal disappeared 24 h post-Dox induction (Fig. 7E). In contrast, in cells co-expressing wild-type DJ-1 and GFP, both DJ-1 and GFP were clearly observed 48 h post-Dox induction (Fig. 7F). These results suggest that destabilized DJ-1 proteins are degraded after mitochondrial translocation. Consistent with this, a recent report found that a number of pathogenic DJ-1 mutants localized in mitochondria undergo intra-mitochondria degradation by LonP1 (Sanchez-Lanzas and Castano, 2021).

We next examined if this degradation is reduced when mitochondrial import is blocked. After Dox-mediated induction, cells were treated with CCCP or valinomycin to inhibit mitochondrial translocation (Fig. 4D). Although the M26I mutant accumulated following CCCP and valinomycin treatment (Fig. 7G, compare lane 2 with lanes 4 and 5), the E18K mutant was barely detectable (Fig. 7G, compare lane 9 with lanes 11 and 12). When the two mutants are compared, the E18K mutation generates a protein that is less stable both in vitro (Figs. 3 and S3) and in cells (Figs. 7B and 7C), and which undergoes more complete mitochondrial localization (Figs. 1 and 3). The results shown in Fig. 7G thus seem contradictory. A clue to understanding this discrepancy was provided by the L10P mutant, although denatured (Fig. 2) it cannot undergo mitochondrial import because of a mutated MTS (Fig. 6). The E18K mutant is similarly denatured but its mitochondrial import is only inhibited following CCCP or valinomycin treatment. Because the L10P mutant undergoes proteasomal degradation (Ramsey and Giasson, 2010; Sanchez-Lanzas and Castano, 2021), we examined the effects of the proteasome inhibitor epoxomicin on mutant DJ-1 protein levels in cells treated with CCCP and valinomycin. Interestingly, epoxomicin failed to inhibit degradation of the E18K mutant (Fig. 7G, lane 10), and only a slight increase in the levels of the mutant protein was observed following CCCP or valinomycin alone (Fig. 7G, lanes 11 and 12). In contrast, a dramatic increase in E18K protein levels was achieved by simultaneous treatment with either uncoupler (CCCP or valinomycin) and the proteasome-inhibitor (Fig. 7G, lanes 13 and 14), indicating that

denatured E18K is usually degraded intra-mitochondria but undergoes proteasomal degradation if cytosolic.

The mitochondrial localization of DJ-1 mutants is reversed by a DJ-1 stabilizer

If protein unfolding is the driving force for the mitochondrial localization of DJ-1, then artificial stabilization should impact DJ-1 localization. We thus examined whether mitochondrial localization of DJ-1 mutants could be blocked with a DJ-1 stabilizer. Using a thermal shift assay, we determined that isatin [a small weight DJ-1 inhibitor that covalently binds to the DJ-1 C106 catalytic center (Tashiro et al., 2018)] stabilizes both WT DJ-1 and the M26I mutant. Isatin interactions caused a slight increase (ΔTm = 1.5°C) in the WT Tm (Figs. 8A, 8D) and a significant increase (ΔTm = 2.5°C) in Tm for the M26I mutant (Figs. 8B, 8D). When *DJ-1* knockout HeLa cells were treated with isatin, the mitochondrial localization of M26I was significantly inhibited (Figs. 8E, 8F). These results though do not rule out the possibility that isatin affects M26I translocation by decreasing $\Delta\Psi m$ similar to CCCP, or that it inhibits some factor that functions in DJ-1 translocation such as the TOMM/TIMM complex. Serendipitously, we found that rather than stabilizing the E18A mutant, isatin actually destabilizes E18A (Figs. 8C, 8D). As such, unlike the M26I mutant, the mitochondrial localization of E18A was unaffected by isatin in *DJ-1* knockout HeLa cells (Figs. 8E, 8F). These results indicate that the compound's effects on the M26I mutant result from protein stabilization rather than via inhibition of a process in mitochondrial translocation, thus supporting our hypothesis that protein unfolding is the driving force underlying DJ-1 mitochondrial localization.

Discussion

A close relationship between neurodegenerative disease and impaired mitochondrial function has been widely recognized. Parkinson's disease is the best-elucidated example with diverse familial Parkinson's disease-associated genes implicated in mitochondrial quality control. One of those genes, *PARK7*, encodes the cytosolic protein DJ-1. Some pathogenic mutations unexpectedly trigger DJ-1 mislocalization from the cytosol to the mitochondrial matrix. Translocation of steady-state cytosolic proteins to the mitochondrial matrix by missense mutations is rare and the underlying mechanism that causes the mitochondrial import has yet to be elucidated.

Mitochondrial translocation of DJ-1 is triggered by several pathogenic mutations such as L166P (Bonifati et al., 2003; Kojima et al., 2016; Maita et al., 2013; Ren et al., 2012). Because other causal gene products for recessive familial Parkinson's disease, PINK1 and Parkin, localize on damaged mitochondria, one might assume that the mechanisms driving the mitochondrial localization of DJ-1, PINK1, and Parkin are similar. However, as a critical point, we want to stress that mitochondrial translocation is not essential for DJ-1 mutants to trigger the onset of Parkinson's disease. In the case of PINK1 and Parkin, their enzymatic activities as a ubiquitin kinase and ubiquitin ligase manifest only on damaged mitochondria (Kane et al., 2014; Kazlauskaite et al., 2014; Koyano et al., 2014; Matsuda et al., 2010; Narendra et al., 2008; Narendra et al., 2010; Okatsu et al., 2015b; Yamano et al., 2016). Indeed, mitochondrial localization is essential for PINK1 and Parkin to exert their genuine functions, inhibition of which promotes Parkinson's disease. Consequently, pathogenic mutations impede their mitochondrial localization. In contrast, various pathogenic mutations in DJ-1 accelerate rather than inhibit mitochondrial localization. The absence of observable mitochondrial stress by mitochondria-localized pathogenic DJ-1 mutants (Fig. S2), however, suggests that they are likely not directly relevant to the onset of Parkinson's disease. Rather, this study demonstrates that destabilized DJ-1 mutants, including several pathogenic mutations (M26I, E163K, and L166P),

translocate to mitochondria, and that a new mitochondrial transport mechanism, which we term "destabilization-dependent mitochondrial import mechanism", drives their mitochondrial localization.

We reported here that the destabilizing effects of various mutations on the DJ-1 protein conformation trigger its translocation to mitochondria. To our knowledge, there are only a few reports of unfolding-dependent mitochondrial translocation. In terms of Parkinson's disease, it is unlikely that pathogenic mitochondrial DJ-1 mutants (such as M26I, E163K, or L166P) exert an effect after transport to the mitochondria. Since these DJ-1 mutants are translocated to mitochondria in response to unfolding, they are likely non-functional and subsequently destined for degradation (Fig. 7). However, if mitochondrial import is only a process in DJ-1 dysfunction, then the question of why DJ-1 has the potential/capacity to undergo mitochondrial translocation remains. As suggested by the fact that mitochondrial translocation of DJ-1 is caused by recessive pathogenic mutations (i.e., loss-of-function mutations), it could be that mitochondrial transport is simply a phenomenon accompanying DJ-1 dysfunction. Conversely, mitochondrial transport might have a positive and significant role on DJ-1. Regarding this topic, we can consider two possibilities. The first possibility is that restricted unfolding and subsequent mitochondrial translocation is essential for the genuine function of DJ-1, and that the DJ-1 MLMs reflect this phenomenon (Fig. 8G, left). As discussed above, the cryptic mitochondrial localization signal at the N-terminus of DJ-1 is essential for the protein to translocate to mitochondria following unfolding. It is possible that some unknown signal or ligand affects the DJ-1 structure restrictedly, and the resulting structural change allows the cryptic N-terminal signal to be exposed. Interestingly, Prahlad et al. reported that E18A, E18N, and E18Q that localize in mitochondria (Fig. 3) are fully dimeric suggesting well-folded, however they are more structurally dynamic and flexible than WT DJ-1 (Prahlad et al., 2014). That

could be consistent with our model, where structural fluctuations in more dynamic mutants transiently expose the N-terminal region and permit mitochondrial import.

A second, and completely different, possibility is that mitochondrial localization of DJ-1 reflects an undetermined mitochondria-based quality control system for cytoplasmic proteins. Interestingly, a similar unfolding-dependent mitochondrial translocation and degradation mechanism, dubbed "MAGIC" (mitochondria as guardian in cytosol), has been reported in yeast (Ruan et al., 2017). In the yeast model, aggregation-prone proteins become disentangled and flood into the mitochondrial matrix. The authors of that study reported on the presence of a similar phenomenon in human RPE-1 (retinal pigment epithelium 1) cells in which a super unstable variant of Flag-tagged luciferase was funneled into the mitochondrial matrix. Data in support of MAGIC in mammalian cells, however, has yet to be further developed. Here, we reported DJ-1 transport into mitochondria via a MAGIC-like mechanism in mammalian cells. As indicated, the reported substrate of mammalian MAGIC was an artificial model protein, and thus DJ-1 could be the first endogenous substrate protein for this mechanism. We believe mutant DJ-1 provides a reproducible and reliable experimental model for exploring MAGIC (which is a novel but not well-accepted idea) in mammalian cells (Fig. 8G, right). This destabilization-dependent import may be the reason why aggregation-prone proteins, such as Aβ and TDP43, have also been reported in mitochondria despite the absence of clear mitochondria-localized signals (Devi et al., 2006; Izumikawa et al., 2017; Manczak et al., 2006; Wang et al., 2016).

Material and Methods

Cell culture and transfection

HeLa cells were cultured at 37°C with 5% CO_2 in Dulbecco's modified Eagle's medium (DMEM, Sigma-Aldrich) containing 1× nonessential amino acids (Gibco), 1× sodium pyruvate (Gibco), and

10% fetal bovine serum (Gibco). HeLa cells used in this study (Cell No. KBN0573-01) were authenticated by JCRB cell bank (Japanese Collection of Research Bioresources Cell Bank) in National Institute of Biomedical Innovation (Osaka, Japan) as they were the same as the HeLa cell registered in ATCC. DJ-1 KO cells were produced using CRISPR as previously described (Kojima et al., 2016). Transfection of plasmids for transient expression was done using the FuGENE6 transfection reagent (Promega) according to the manufacturer's protocol.

Immunocytochemistry

Cells were fixed with 4% paraformaldehyde, permeabilized in 1% Triton X-100 or 50 μg/mL digitonin for 15 min, diluted in blocking solution (0.1% gelatin in PBS), blocked for 30 min, and stained with the following primary antibodies: an anti-TOMM20 antibody FL-145 (Santa Crus Biotech., 1:2,000), an anti-Hsp60 antibody N20 (Santa Crus Biotech., 1:250), or an anti-HA antibody TANA2 (MBL, 1:1,000). Among the secondary antibodies used were an Alexa Fluor 488-, 568-, or 647-conjugated anti-mouse IgG or an anti-rabbit IgG antibody (Thermo Fisher Scientific, 1:2,000). Cells were imaged using a laser-scanning microscope (LSM710 or LSM780; Carl Zeiss). Antibodies used in this study and their Research Resource Identifiers (RRIDs) are listed in Supplementary Table 1.

Uncoupler treatment to depolarize mitochondria

To examine whether the mitochondrial transport of the DJ-1 E18K mutant and DJ17-SNCA depends on ΔΨm, HeLa cells were pre-treated with 10 μM CCCP or 10 μM valinomycin for 2 h before transfection, and then the plasmid encoding the DJ-1 E18K mutant or DJ17-SNCA was introduced. Cells were further incubated for 20 h in the presence of CCCP or valinomycin, and the subcellular localization of DJ-1 E18K or DJ17-SNCA was examined.

siRNA analyses

For siRNA analysis, the siGENOME siRNA SMART pool TIMM23 (M-190121-00, Thermo Fisher Scientific) and siGENOME siRNA SMART pool TOMM40 (M-012732-00, Thermo Fisher Scientific) were used for knockdown of TIMM23 and TOMM40, respectively. As a control, the siGENOME Control siRNA pool (D-001206-13-20, Thermo Fisher Scientific) was used. 10 nM TIMM23, TOMM40, and control siRNAs were introduced into HeLa cells using Lipofectamine RNAiMAX (Life Technologies). At 24 h post-siRNA transfection, the cells were re-seeded on 35 mm glass bottom dishes (MatTek Corporation), and then either Su9-GFP, DJ-1(WT), DJ-1(E18K), or DJ-1(E18H) plasmids were transfected using Fugene 6 (Promega). The resulting cells were incubated for another 24 h and then subjected to immunocytochemical analysis. For statistical analyses, cells were categorized based on the degree of DJ-1 or Su9-GFP mitochondrial co-localization. These analyses were carried out using 100 cells per siRNA condition. Error bars represent the mean ± SD of three independent experiments.

Accessible Surface Area (ASA) Determination

To determine the ASA value for each residue in the DJ-1 mitochondria localized mutants, we used the methods described in Ahmad et al (Ahmad et al., 2004). The DJ-1 crystal structure (PDB: 1P5F) was used as a template for value determination.

Recombinant protein purification

To obtain recombinant DJ-1 proteins from *E. coli*, WT and mutant DJ-1 genes were sub-cloned into pET21a(+) and pET28a(+) plasmids (Novagen - Merck Millipore), and then transformed into the *E. coli* strain BL21(DE3)+RIL (Agilent Technologies). His6-tagged WT DJ-1 and various DJ-1 mutants were purified by standard procedures using nickel-agarose (Ni-NTA Agarose, Qiagen) and an elution buffer [200 mM NaCl, 10 mM 2-mercaptoethanol, and 500 - 750 mM imidazole in 20

mM sodium phosphate buffer (pH 7.0)]. Recombinant DJ-1 proteins were dialyzed using 20 mM sodium phosphate buffer (pH 7.0) supplemented with 200 mM NaCl ± 10% glycerol, and stored at -80 °C. The WT and mutant DJ-1 were subjected to SDS-PAGE followed by CBB staining to confirm that the purified proteins resolved as single bands.

Recombinant chimera proteins (DJ17-GFP and DJ17-SNCA) were prepared as follows. *Escherichia coli* BL21-CodonPlus(DE3)-RIL competent cells (Agilent Technologies) transformed with pGEX-6P-1 plasmid encoding GST-DJ17-GFP or GST-DJ17-SNCA were grown in LB medium supplemented with 100 µg/ml ampicillin and 25 µg/ml chloramphenicol at 37°C. Expression of GST-DJ17-GFP and GST-DJ17-SNCA were induced by addition of 200 µM IPTG for 16hrs at 18°C. The bacterial cell pellets after centrifugation were resuspended in TBS buffer (50 mM Tris-HCl pH7.5, 120 mM NaCl) supplemented with lysozyme, DNAse I, DTT, MgCl2, and protease inhibitor cocktail. The obtained cell suspension was sonicated (Advanced-Digital Sonifer, Branson), and insoluble proteins were removed by centrifugation. The supernatants were mixed with equilibrated glutathione-Sepharose 4B (GE Healthcare) for 40 min at 4°C. The sepharose was then loaded onto a column and washed with TBS buffer containing 1 mM Tris(2-carboxylethl)phosphine (TCEP; Sigma). The bound chimera proteins (DJ17-GFP and DJ17-SNCA) were eluted from glutathione-Sepharose 4B with 1.5 ml TBS buffer containing 1 mM TECP and 20 units Prescission protease (GE Healthcare), and were subjected to the thermal shift analysis.

Partial trypsin digestion

Recombinant DJ-1 (11 µM) was incubated with Trypsin Gold (1 µg/mL) in 200mM Tris-HCl (pH 8.0) buffer solution at 37℃ for 22 h. Samples were then mixed with 2x protease inhibitor and loading buffer, followed by denaturation at 98℃ for 10 min. Samples were separated in a 12% acrylamide gel, followed by fixation and Comassie Brilliant Blue staining. The bands were digitized

with an ImageQuant LAS LAS4000 (GE healthcare) and band intensity was determined using Image J software.

Thermal shift assay

Determination of thermal stability of recombinant protein was done using Protein Thermal Shift Dye (Thermo Fisher Scientific). DJ-1 and chimeric proteins (30 μM) were incubated in the reaction buffer containing 0.01% thermal shift dye according to the manufacturer's protocol. Fluorescence was measured using the ROX channel of a BioRad CFX96 Real Time PCR, with a 0.5°C/15s per step (20-95°C) melting curve. To measure isatin-mediated stabilization, 500 μM of isatin (Tokyo Chemical Industry Co.) was added after all the other reagents were mixed. Peaks were determined using BioRad CFX Manager software.

Isatin treatment in cells

To test if isatin affected the subcellular localization of DJ-1, HeLa DJ-1 KO cells were transiently transfected with plasmids expressing DJ-1 E18A or M26I mutants. After 4 h, 500 μM isatin (Tokyo Chemical Industry Co.) was added to media. After 16 h, the cells were fixed and subjected to immunocytochemistry as previously described.

Immunoblot analysis

Cell lysates were collected in TNE-N+ buffer (150 mM NaCl, 20 mM Tris-HCl, pH 8.0, 1 mM EDTA, and 1% NP-40) in the presence of various inhibitors. To detect the indicated proteins, anti-Flag antibody FLA1 (MBL), anti-DJ-1 antibody 3E8 (MBL), anti-Tubulin antibody YL1/2 (Abcam), anti-HA antibody TANA2 (MBL), anti-TOMM40 antibody (a gift from Dr. Toshihiko Oka), anti-TIMM23 antibody (BD Biosciences), anti-TOMM20 antibody (Proteintech), anti-OPA1 antibody (BD Biosciences), anti-PGAM5 antibody (Abcam), anti-ATF4 antibody (CST), anti-Actin antibody

C4 (Merck Millipore) or an anti-GFP antibody ab6556 (Abcam) were used as primary antibodies, and HRP-conjugated goat anti-mouse IgG or anti-rabbit IgG antibody was used as secondary antibodies (Jackson ImmunoResearch). The HRP substrate consisted of the Western Lightning Plus-ECL (PerkinElmer) and images were captured on an ImageQuant LAS4000 (GE healthcare). Quantification was done using Image J software. Antibodies used in this study and their Research Resource Identifiers (RRIDs) are listed in Supplementary Table 1. To provide cellular stress in Fig. S2, WT HeLa cells were treated with DMSO (NT: non-treated), 10 μM valinomycin (val) or 300 nM thapsigargin (TG) for 3hrs, and then total cell lysates were prepared for immunoblotting.

Doxycycline-induced chase

A pTRE-IRES plasmid (Takara Bio USA) was used to simultaneously express DJ-1 and EGFP, which are separated by the IRES (internal ribosome entry site), following the addition of doxycycline. Cells were transfected with the same amount of pTET3G (Takara Bio USA) and the appropriate pTRE-IRES plasmids. After 24 h, media containing 50 ng/mL doxycycline (Dox) was added to initiate expression of EGFP and DJ-1 for 24 h. Cells were then washed and re-plated in media without doxycycline. This time point was considered day 0, and the time was counted forward as day +1 and +2. To assess the degradation process of DJ-1 in detail, cells were treated with 10 μM CCCP, 10 μM valinomycin, and/or 2 μM epoxomicin following Dox-mediated induction.

Statistical analysis

For quantitative co-localization and statistical analysis, the co-localization of TOMM20 with various DJ-1 mutants or chimera proteins (e.g., DJ17-GFP and DJ17-SNCA) was calculated using Zen software (Carl Zeiss) as a Pearson correlation coefficient. In the associated box-plots of the data, the dots indicate individual Pearson correlation coefficient data points for each cell, the center

lines indicate the medians, the box limits indicate the 25th and 75th percentiles as determined by the R software package, and whiskers extend 1.5 times the interquartile range from the 25th and 75th percentiles. Outliers are represented by dots outside of the whiskers, mean values are shown on the boxes, and the number of samples is indicated above the X-axis. Statistical significance was calculated using one-way ANOVA in GraphPad Prism 6. For one-way ANOVA experiments, the Sidak correction for multiple comparisons was used. Differences were considered significant at $p < 0.01$.

Data availability statement

The authors declare that all materials are available to readers with due qualifications in material transfer agreements, and all data are available upon reasonable request from the corresponding author.

Acknowledgements

We would like to thank the help of Drs. Junjiro Horiuchi, Daisuke Yamane (TMIMS, Japan) and Mark Wilson (University of Nebraska, USA) for their constructive discussions during manuscript preparation. We also thank Dr. Toshihiko Oka for anti-TOMM40 antibody. This work was supported by JSPS KAKENHI Grant Numbers JP18H02443 (to N.M.), JP17J03737 (to W.K.), JP16K21680 and JP18K11543 (to K.I.), JP16K18545, JP18H05500 and JP18K06237 (to K.Y.), 16H02420 (to K.Tsumoto), JP26000014 (to K.Tanaka), and JP16F15387 (to B.B.Q.); by JSPS PRESTO and the Chieko Iwanaga Fund for Parkinson's Disease Research (to N.M.); by AMED Platform Project of Basis for Supporting Innovative Drug Discovery and Life Science Research (BINDS) Grant Number JP21am0101114 (to K.I., C.M. and T.H.); by International Research Fellow of the JSPS (to B.B.Q.); by MEXT Platform for Drug Discovery, Informatics and Structural Life Science (to K.Tsumoto); and by the Takeda Science Foundation (to K.Tanaka and N.M.).

Author Contributions

This part was described according to the Contributor Roles Taxonomy (CrediT):

Conceptualization: BBQ, WK, and NM. Funding acquisition: TH, KT, KY, KT, and NM. Investigation: BBQ, WK, MK, CU, and KY. Methodology: BBQ, KI, CM, CU, TH, ST, JMMC, and NM. Project administration: TH, KT, KY, KT, and NM. Resource: MK, ST, and JMMC. Supervision: TH, KT, KT, and NM. Visualization: BBQ, WK, MK, KI, KY, and NM. Writing – original draft: BBQ and NM. Writing—review and editing: WK, KI, CM, TH, KT, KY, and KT.

Author Information

Correspondence and requests for materials should be addressed to matsuda-nr@igakuken.or.jp

Competing interests

Authors declare that there is no financial or competing interests regarding the presented research in this manuscript.

References

Ahmad, S., Gromiha, M., Fawareh, H. and Sarai, A. (2004). ASAView: database and tool for solvent accessibility representation in proteins. *BMC Bioinformatics* **5**, 51.

Anand, R., Wai, T., Baker, M. J., Kladt, N., Schauss, A. C., Rugarli, E. and Langer, T. (2014). The i-AAA protease YME1L and OMA1 cleave OPA1 to balance mitochondrial fusion and fission. *J Cell Biol* **204**, 919-29.

Bjorkblom, B., Maple-Grodem, J., Puno, M. R., Odell, M., Larsen, J. P. and Moller, S. G. (2014). Reactive oxygen species-mediated DJ-1 monomerization modulates intracellular trafficking involving karyopherin beta2. *Mol Cell Biol* **34**, 3024-40.

Blackinton, J., Lakshminarasimhan, M., Thomas, K. J., Ahmad, R., Greggio, E., Raza, A. S., Cookson, M. R. and Wilson, M. A. (2009). Formation of a stabilized cysteine sulfinic acid is critical for the mitochondrial function of the parkinsonism protein DJ-1. *J Biol Chem* **284**, 6476-85.

Bonifati, V., Rizzu, P., van Baren, M. J., Schaap, O., Breedveld, G. J., Krieger, E., Dekker, M. C., Squitieri, F., Ibanez, P., Joosse, M. et al. (2003). Mutations in the DJ-1 gene associated with autosomal recessive early-onset parkinsonism. *Science* **299**, 256-9.

Cali, T., Ottolini, D., Soriano, M. E. and Brini, M. (2015). A new split-GFP-based probe reveals DJ-1 translocation into the mitochondrial matrix to sustain ATP synthesis upon nutrient deprivation. *Hum Mol Genet* **24**, 1045-60.

Canet-Aviles, R. M., Wilson, M. A., Miller, D. W., Ahmad, R., McLendon, C., Bandyopadhyay, S., Baptista, M. J., Ringe, D., Petsko, G. A. and Cookson, M. R. (2004). The Parkinson's disease protein DJ-1 is neuroprotective due to cysteine-sulfinic acid-driven mitochondrial localization. *Proc Natl Acad Sci U S A* **101**, 9103-8.

Devi, L., Prabhu, B. M., Galati, D. F., Avadhani, N. G. and Anandatheerthavarada, H. K. (2006). Accumulation of amyloid precursor protein in the mitochondrial import channels of human Alzheimer's disease brain is associated with mitochondrial dysfunction. *J Neurosci* **26**, 9057-68.

Fukasawa, Y., Tsuji, J., Fu, S. C., Tomii, K., Horton, P. and Imai, K. (2015). MitoFates: improved prediction of mitochondrial targeting sequences and their cleavage sites. *Mol Cell Proteomics* **14**, 1113-26.

Hartl, F. U., Pfanner, N., Nicholson, D. W. and Neupert, W. (1989). Mitochondrial protein import. *Biochim Biophys Acta* **988**, 1-45.

Honbou, K., Suzuki, N. N., Horiuchi, M., Niki, T., Taira, T., Ariga, H. and Inagaki, F. (2003). The crystal structure of DJ-1, a protein related to male fertility and Parkinson's disease. *J Biol Chem* **278**, 31380-4.

Ishihara, N., Fujita, Y., Oka, T. and Mihara, K. (2006). Regulation of mitochondrial morphology through proteolytic cleavage of OPA1. *EMBO J* **25**, 2966-77.

Izumikawa, K., Nobe, Y., Yoshikawa, H., Ishikawa, H., Miura, Y., Nakayama, H., Nonaka, T., Hasegawa, M., Egawa, N., Inoue, H. et al. (2017). TDP-43 stabilises the processing intermediates of mitochondrial transcripts. *Sci Rep* **7**, 7709.

Kane, L. A., Lazarou, M., Fogel, A. I., Li, Y., Yamano, K., Sarraf, S. A., Banerjee, S. and Youle, R. J. (2014). PINK1 phosphorylates ubiquitin to activate Parkin E3 ubiquitin ligase activity. *J Cell Biol* **205**, 143-53.

Kazlauskaite, A., Kondapalli, C., Gourlay, R., Campbell, D. G., Ritorto, M. S., Hofmann, K., Alessi, D. R., Knebel, A., Trost, M. and Muqit, M. M. (2014). Parkin is activated by PINK1-dependent phosphorylation of ubiquitin at Ser65. *Biochem J* **460**, 127-39.

Kojima, W., Kujuro, Y., Okatsu, K., Bruno, Q., Koyano, F., Kimura, M., Yamano, K., Tanaka, K. and Matsuda, N. (2016). Unexpected mitochondrial matrix localization of Parkinson's disease-related DJ-1 mutants but not wild-type DJ-1. *Genes Cells* **21**, 772-88.

Koyano, F., Okatsu, K., Kosako, H., Tamura, Y., Go, E., Kimura, M., Kimura, Y., Tsuchiya, H., Yoshihara, H., Hirokawa, T. et al. (2014). Ubiquitin is phosphorylated by PINK1 to activate parkin. *Nature* **510**, 162-6.

Lo, M. C., Aulabaugh, A., Jin, G., Cowling, R., Bard, J., Malamas, M. and Ellestad, G. (2004). Evaluation of fluorescence-based thermal shift assays for hit identification in drug discovery. *Anal Biochem* **332**, 153-9.

Maita, C., Maita, H., Iguchi-Ariga, S. M. and Ariga, H. (2013). Monomer DJ-1 and its N-terminal sequence are necessary for mitochondrial localization of DJ-1 mutants. *PLoS One* **8**, e54087.

Manczak, M., Anekonda, T. S., Henson, E., Park, B. S., Quinn, J. and Reddy, P. H. (2006). Mitochondria are a direct site of A beta accumulation in Alzheimer's disease neurons: implications for free radical generation and oxidative damage in disease progression. *Hum Mol Genet* **15**, 1437-49.

Matsuda, N., Sato, S., Shiba, K., Okatsu, K., Saisho, K., Gautier, C. A., Sou, Y. S., Saiki, S., Kawajiri, S., Sato, F. et al. (2010). PINK1 stabilized by mitochondrial depolarization recruits Parkin to damaged mitochondria and activates latent Parkin for mitophagy. *J Cell Biol* **189**, 211-21.

Nagakubo, D., Taira, T., Kitaura, H., Ikeda, M., Tamai, K., Iguchi-Ariga, S. M. and Ariga, H. (1997). DJ-1, a novel oncogene which transforms mouse NIH3T3 cells in cooperation with ras. *Biochem Biophys Res Commun* **231**, 509-13.

Narendra, D., Tanaka, A., Suen, D. F. and Youle, R. J. (2008). Parkin is recruited selectively to impaired mitochondria and promotes their autophagy. *J Cell Biol* **183**, 795-803.

Narendra, D. P., Jin, S. M., Tanaka, A., Suen, D. F., Gautier, C. A., Shen, J., Cookson, M. R. and Youle, R. J. (2010). PINK1 is selectively stabilized on impaired mitochondria to activate Parkin. *PLoS Biol* **8**, e1000298.

Nural, H., He, P., Beach, T., Sue, L., Xia, W. and Shen, Y. (2009). Dissembled DJ-1 high molecular weight complex in cortex mitochondria from Parkinson's disease patients. *Mol Neurodegener* **4**, 23.

Okatsu, K., Kimura, M., Oka, T., Tanaka, K. and Matsuda, N. (2015a). Unconventional PINK1 localization to the outer membrane of depolarized mitochondria drives Parkin recruitment. *J Cell Sci* **128**, 964-78.

Okatsu, K., Koyano, F., Kimura, M., Kosako, H., Saeki, Y., Tanaka, K. and Matsuda, N. (2015b). Phosphorylated ubiquitin chain is the genuine Parkin receptor. *J Cell Biol* **209**, 111-28.

Olzmann, J. A., Brown, K., Wilkinson, K. D., Rees, H. D., Huai, Q., Ke, H., Levey, A. I., Li, L. and Chin, L. S. (2004). Familial Parkinson's disease-associated L166P mutation disrupts DJ-1 protein folding and function. *J Biol Chem* **279**, 8506-15.

Ormo, M., Cubitt, A. B., Kallio, K., Gross, L. A., Tsien, R. Y. and Remington, S. J. (1996). Crystal structure of the Aequorea victoria green fluorescent protein. *Science* **273**, 1392-5.

Prahlad, J., Hauser, D. N., Milkovic, N. M., Cookson, M. R. and Wilson, M. A. (2014). Use of cysteine-reactive cross-linkers to probe conformational flexibility of human DJ-1 demonstrates that Glu18 mutations are dimers. *J Neurochem* **130**, 839-53.

Quiros, P. M., Prado, M. A., Zamboni, N., D'Amico, D., Williams, R. W., Finley, D., Gygi, S. P. and Auwerx, J. (2017). Multi-omics analysis identifies ATF4 as a key regulator of the mitochondrial stress response in mammals. *J Cell Biol* **216**, 2027-2045.

Ramsey, C. P. and Giasson, B. I. (2010). L10p and P158DEL DJ-1 mutations cause protein instability, aggregation, and dimerization impairments. *J Neurosci Res* **88**, 3111-24.

Ren, H., Fu, K., Mu, C., Zhen, X. and Wang, G. (2012). L166P mutant DJ-1 promotes cell death by dissociating Bax from mitochondrial Bcl-XL. *Mol Neurodegener* **7**, 40.

Ruan, L., Zhou, C., Jin, E., Kucharavy, A., Zhang, Y., Wen, Z., Florens, L. and Li, R. (2017). Cytosolic proteostasis through importing of misfolded proteins into mitochondria. *Nature* **543**, 443-446.

Sanchez-Lanzas, R. and Castano, J. G. (2021). Mitochondrial LonP1 protease is implicated in the degradation of unstable Parkinson's disease-associated DJ-1/PARK 7 missense mutants. *Sci Rep* **11**, 7320.

Sekine, S., Kanamaru, Y., Koike, M., Nishihara, A., Okada, M., Kinoshita, H., Kamiyama, M., Maruyama, J., Uchiyama, Y., Ishihara, N. et al. (2012). Rhomboid protease PARL mediates the mitochondrial membrane potential loss-induced cleavage of PGAM5. *J Biol Chem* **287**, 34635-45.

Semisotnov, G. V., Rodionova, N. A., Razgulyaev, O. I., Uversky, V. N., Gripas, A. F. and Gilmanshin, R. I. (1991). Study of the "molten globule" intermediate state in protein folding by a hydrophobic fluorescent probe. *Biopolymers* **31**, 119-28.

Tao, X. and Tong, L. (2003). Crystal structure of human DJ-1, a protein associated with early onset Parkinson's disease. *J Biol Chem* **278**, 31372-9.

Tashiro, S., Caaveiro, J. M. M., Nakakido, M., Tanabe, A., Nagatoishi, S., Tamura, Y., Matsuda, N., Liu, D., Hoang, Q. Q. and Tsumoto, K. (2018). Discovery and Optimization of Inhibitors of the Parkinson's Disease Associated Protein DJ-1. *ACS Chem Biol* **13**, 2783-2793.

Theillet, F. X., Binolfi, A., Bekei, B., Martorana, A., Rose, H. M., Stuiver, M., Verzini, S., Lorenz, D., van Rossum, M., Goldfarb, D. et al. (2016). Structural disorder of monomeric alpha-synuclein persists in mammalian cells. *Nature* **530**, 45-50.

Wang, W., Wang, L., Lu, J., Siedlak, S. L., Fujioka, H., Liang, J., Jiang, S., Ma, X., Jiang, Z., da Rocha, E. L. et al. (2016). The inhibition of TDP-43 mitochondrial localization blocks its neuronal toxicity. *Nat Med* **22**, 869-78.

Wilson, M. A., Collins, J. L., Hod, Y., Ringe, D. and Petsko, G. A. (2003). The 1.1-A resolution crystal structure of DJ-1, the protein mutated in autosomal recessive early onset Parkinson's disease. *Proc Natl Acad Sci U S A* **100**, 9256-61.

Wilson, M. A., Ringe, D. and Petsko, G. A. (2005). The atomic resolution crystal structure of the YajL (ThiJ) protein from Escherichia coli: a close prokaryotic homologue of the Parkinsonism-associated protein DJ-1. *J Mol Biol* **353**, 678-91.

Xu, J., Zhong, N., Wang, H., Elias, J. E., Kim, C. Y., Woldman, I., Pifl, C., Gygi, S. P., Geula, C. and Yankner, B. A. (2005). The Parkinson's disease-associated DJ-1 protein is a transcriptional co-activator that protects against neuronal apoptosis. *Hum Mol Genet* **14**, 1231-41.

Yamano, K., Matsuda, N. and Tanaka, K. (2016). The ubiquitin signal and autophagy: an orchestrated dance leading to mitochondrial degradation. *EMBO Rep* **17**, 300-16.

Zhang, L., Shimoji, M., Thomas, B., Moore, D. J., Yu, S. W., Marupudi, N. I., Torp, R., Torgner, I. A., Ottersen, O. P., Dawson, T. M. et al. (2005). Mitochondrial localization of the Parkinson's disease related protein DJ-1: implications for pathogenesis. *Hum Mol Genet* **14**, 2063-73.

Figures

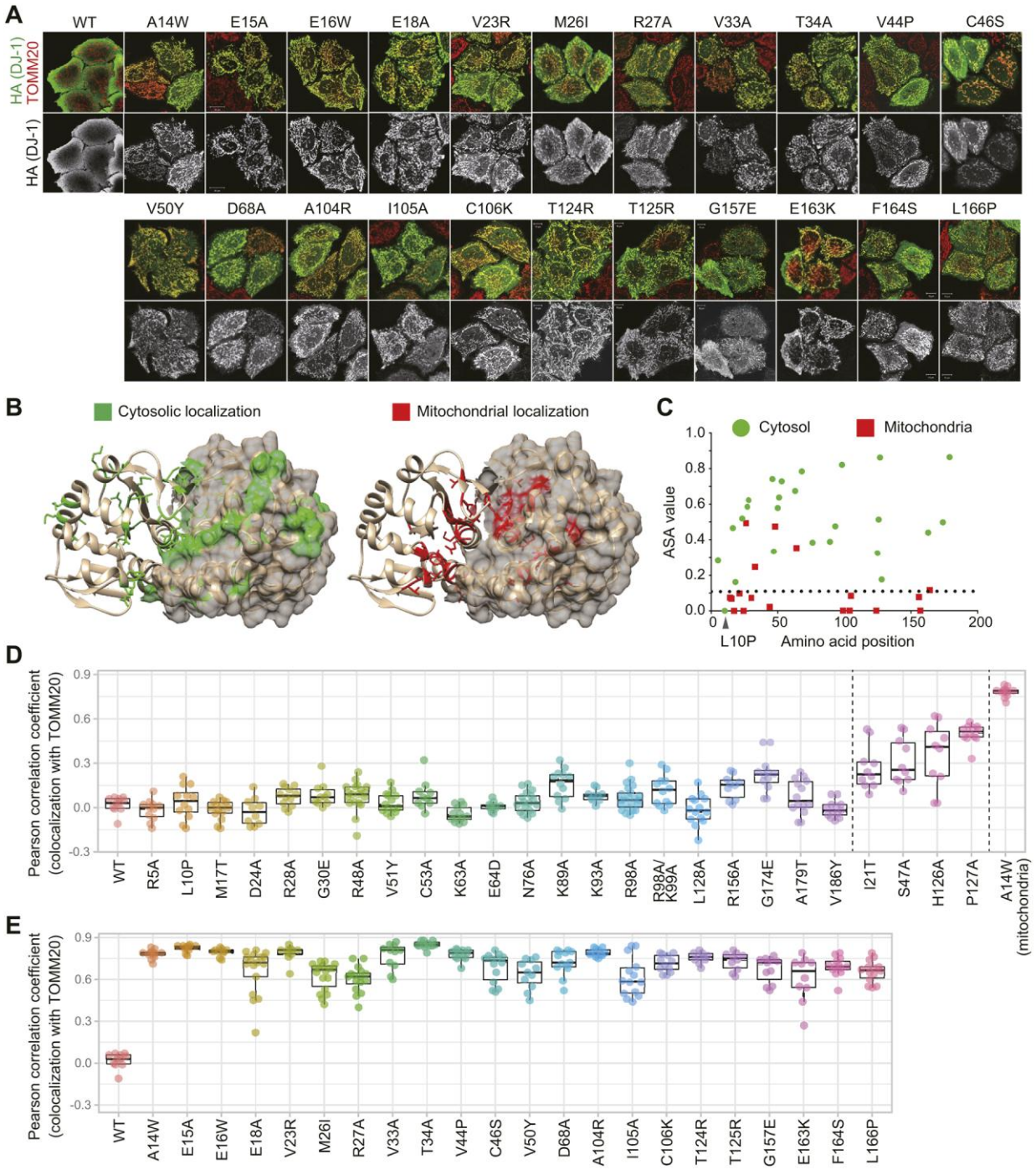

Fig. 1 –Mutations buried in the DJ-1 structure responsible for mitochondrial localization.

(A) Mitochondrial localization of newly identified DJ-1 mutants. Top images - merged images for the DJ-1 constructs (green) and the mitochondrial marker TOMM20 (red) in *DJ-1* knockout cells;

bottom images - DJ-1 constructs alone. Representative images of two independent experiments are shown. (B) Location of the mutation sites in relation to the DJ-1 dimer structure are shown. One DJ-1 monomer is shown in ribbon format, whereas the other is shown in surface mode. (C) Values for the accessible surface area (ASA), equivalent to solvent accessibility of each amino acid, are shown. Amino acid sites linked to mitochondrial localization are shown in red, whereas those associated with cytosolic localization are shown in green. With the exception of L10P, all of the DJ-1 mutations in the buried structure (ASA value < 0.1) cause mitochondrial localization. (D) and (E); For quantitative analysis, the co-localization of DJ-1 mutants with the mitochondrial marker TOMM20 was calculated as a Pearson correlation coefficient in individual cells - (D) Cytosolic DJ-1 mutants, (E) Mitochondrial mutants.

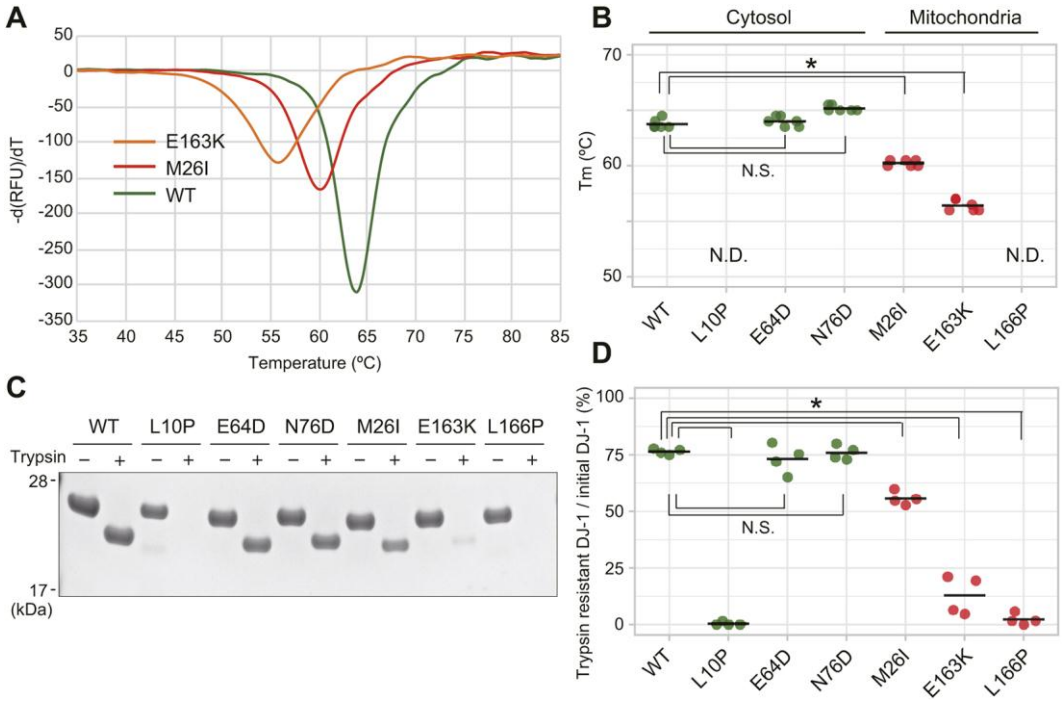

Fig. 2 –Folding instability of DJ-1 pathogenic mutants determines their mitochondrial localization. (A) and (B): The melting temperatures (Tm) of N-terminal 6xHis-tagged DJ-1 proteins were measured via a thermal shift assay. Representative thermal spectra are shown in (A), and averaged Tm with individual data points of three independent experiments are shown in (B). Mitochondria-localized pathogenic DJ-1 mutants are characterized by a higher Tm. No Tm could be determined for the L10P mutation, suggesting the absence of any structure. Asterisk indicates $P < 0.01$ in one way ANOVA, N.S., not significant. (C) and (D): Folding stability of DJ-1 pathogenic mutants under physiological temperature (37°C) assessed via trypsin digestion. Recombinant 6xHis-DJ-1 proteins with the indicated pathogenic mutations were incubated in the presence or absence of trypsin. (C) Representative immunoblotting data of two independent experiments are shown. (D) Degree of trypsin susceptibility after incubation for 22 h. Individual data points of two independent experiments are shown. In (B) and (D), asterisk indicates $P < 0.01$ in one way ANOVA, N.S., not significant as $P > 0.01$.

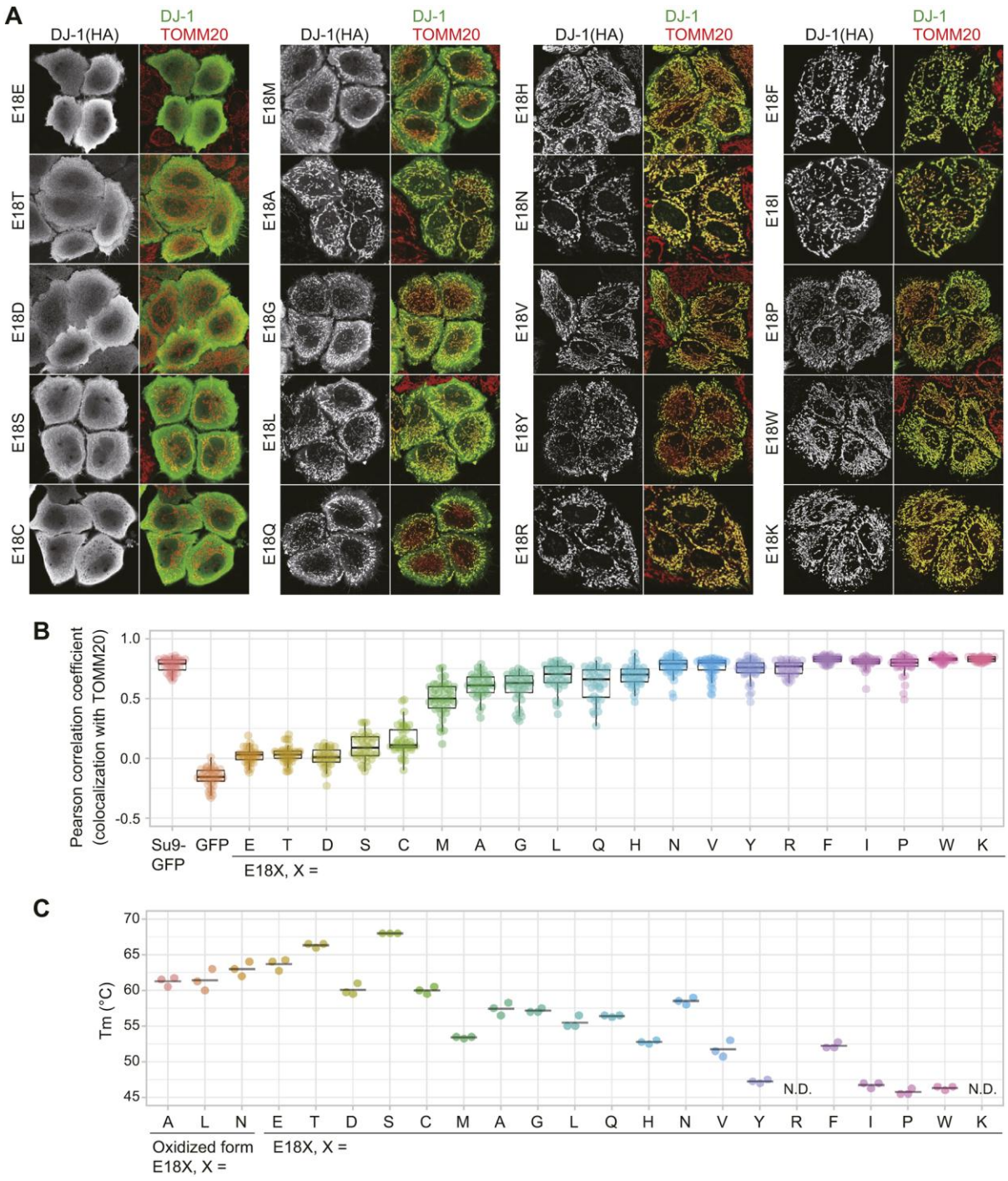

Fig. 3 –Folding stability of DJ-1 E18X mutants.

(A) Systematic substitution of the E18 residue in DJ-1 leads to varied subcellular localization. Representative images of two independent experiments for the DJ-1 E18X (X indicates optional amino acid) mutants are shown. The left figures show localization of the DJ-1 constructs and the right figures show merged images for the DJ-1 constructs (green) and the mitochondrial marker

TOMM20 (red) in *DJ-1* knockout cells. (B) The Pearson correlation coefficients for co-localization of the DJ-1 E18X mutants with TOMM20 were calculated in individual cells. Su9-GFP and GFP are representative mitochondrial and cytosolic marker proteins. Individual data points of two independent experiments are shown. (C) Melting temperatures for the C-terminal 6xHis-tagged E18X mutants were determined via thermal shift assays as in Fig. 2. Individual data points of three independent experiments and the averaged Tm for each construct are shown.

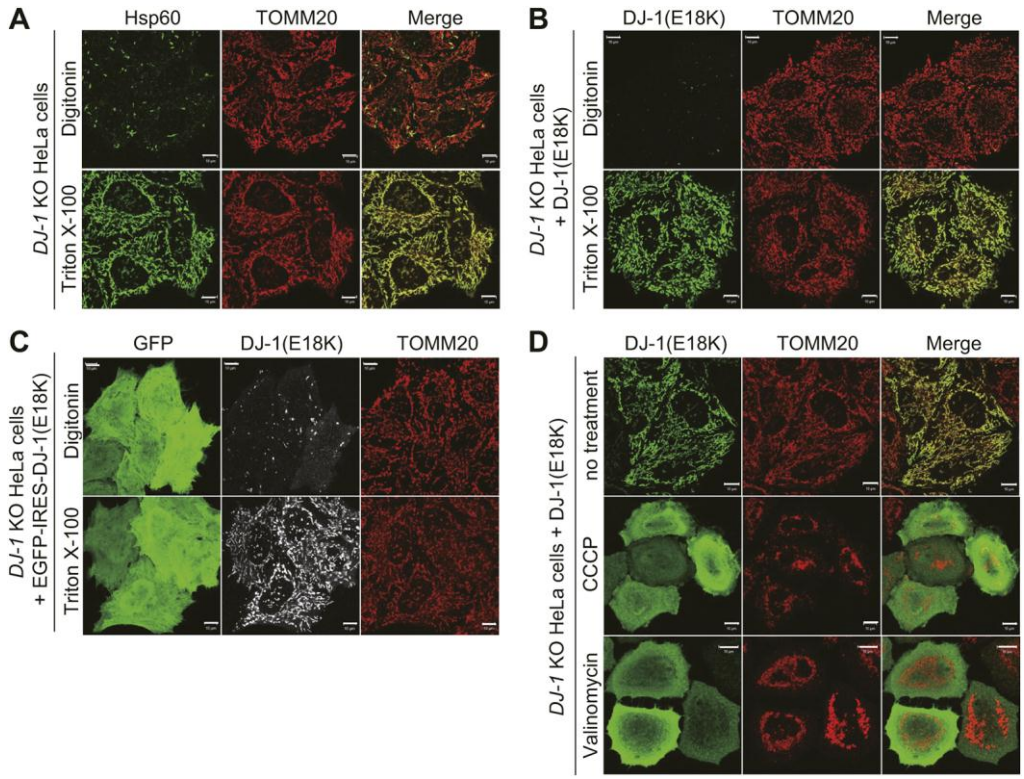

Fig. 4 –The DJ-1 E18K mutant is translocated into the mitochondrial matrix.

(A) Permeabilization with digitonin was insufficient for detecting the matrix protein Hsp60, instead permeabilization with Triton X-100 was required. In contrast, the outer mitochondrial membrane protein TOMM20 was observed irrespective of the permeabilization conditions. (B) *DJ-1* KO HeLa cells expressing an HA-tagged DJ-1 E18K mutant were immunostained with an anti-HA antibody after permeabilization with digitonin or Triton X-100. Detection of the DJ-1 E18K mutant requires Triton X-100 permeabilization. (C) To confirm that the DJ-1 E18K mutant was expressed in digitonin-permeabilized cells, a GFP-IRES-DJ-1(E18K) plasmid was transfected and subjected to immunocytochemistry as in (B). (D) *DJ-1* KO HeLa cells were pre-treated with 10 μM valinomycin or 15 μM CCCP prior to transfecting HA-tagged DJ-1 E18K. The subcellular localization was determined using anti-HA and anti-TOMM20 antibodies. Valinomycin and CCCP treatment inhibited mitochondrial localization of the DJ-1 E18K mutant. Data shown in Fig. 4 indicate that DJ-1 is transported across the inner mitochondrial membrane. White bars, 10 μm. Reproducibility of these results were confirmed by independent experiments.

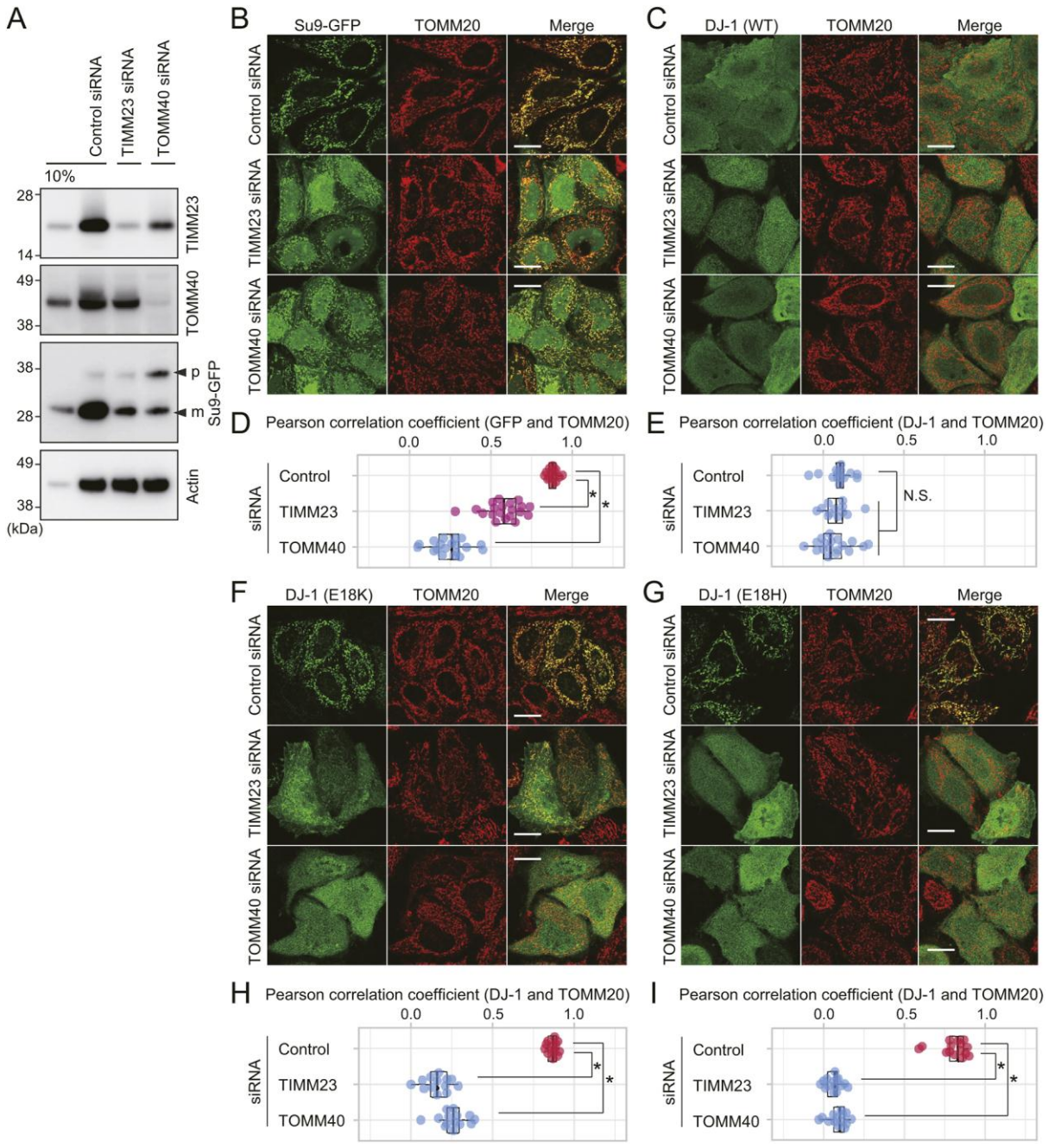

Fig. 5 – Import of the DJ-1 mutants requires mitochondrial protein translocases TOMM40 and TIMM23

(A) siRNA-mediated reduction in expression of endogenous TIMM23 and TOMM40. *DJ-1* KO HeLa cells expressing Su9-GFP were treated with control, TIMM23, or TOMM40 siRNAs, and then immunoblotted using the indicated antibodies. To assess the knock-down efficiency, 10% of the control siRNA treated cell lysate was also loaded. The precursor and mature forms of Su9-GFP

are shown as p and m. Immunoblots are representative of two independent experiments. In (B) and (C), *DJ-1* KO HeLa cells pre-treated with control, TIMM23, or TOMM40 siRNA were transfected with Su9-GFP (B) or WT DJ-1 (C), and then subjected to immunocytochemistry. For quantitative analysis in (D) and (E), the co-localization of GFP or DJ-1 with TOMM20 was calculated as a Pearson correlation coefficient in individual cells with quantitative analyses done using data in (B) and (C). In (F) to (I), *DJ-1* KO HeLa cells pre-treated with control, TIMM23, or TOMM40 siRNA were transfected with E18K (F and H) or E18H (G and I) DJ-1 mutants and then subjected to immunocytochemical and quantitative analyses as in (B-E). Asterisk in (D), (H), or (I) indicates statistically significant differences from control. Asterisk indicates $P < 0.01$ in one way ANOVA, N.S., not significant as $P > 0.01$. Representative images of two independent experiments are shown in (B), (C), (F), and (G). White bars, 10 μm.

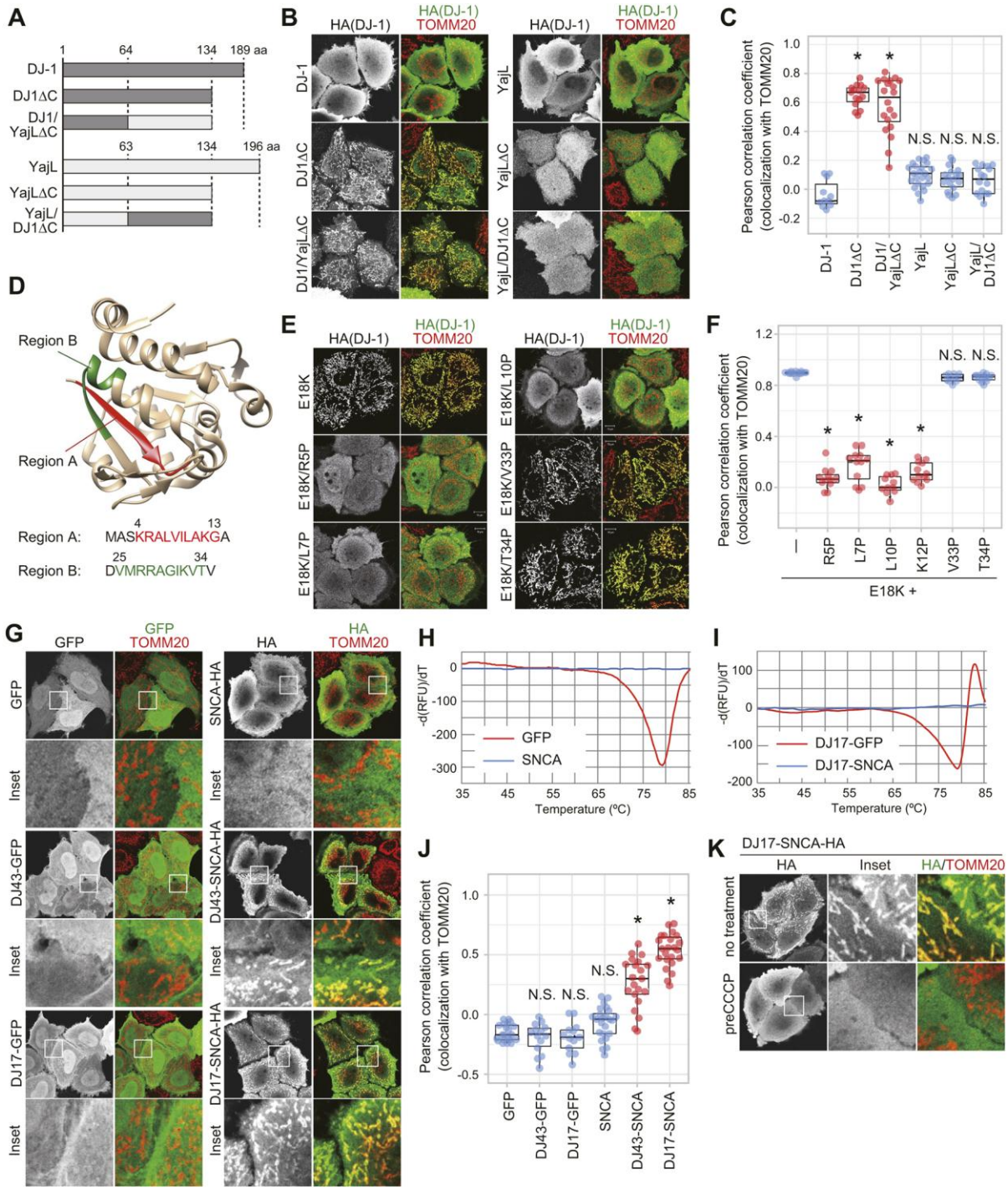

Fig. 6 –DJ-1 has a cryptic N-terminal MTS that is essential for mitochondrial localization.

(A) Schematic diagram of the DJ-1 and YajL chimeric constructs. (B) Subcellular localization of the chimeric proteins in *DJ-1* knockout cells. (C) Quantitative analysis of data shown in (B), the co-localization of various chimeric proteins with the mitochondrial marker TOMM20 was calculated

as a Pearson correlation coefficient in individual cells. (D) Sequence of regions A (red) and B (green) and their location in the DJ-1 structure. Those regions were detected by PA score (Positively charged Amphiphilicity score) used in MitoFates. (E) Pro substitutions in region A of the E18K mutant inhibit mitochondrial localization in *DJ-1* knockout cells, whereas the same substitutions in region B had no effect on mitochondrial localization. (F) Quantitative analysis of data shown in (E), the co-localization of DJ-1 mutants with TOMM20 was calculated as a Pearson correlation coefficient in individual cells. (G) The subcellular localization of GFP and SNCA (α-synuclein) when fused with amino acids 1-43 (DJ43) or 1-17 (DJ17) of DJ-1. SNCA is targeted to the mitochondria when fused with the DJ-1 MTS, whereas the same MTS had no effect on GFP localization. (H) and (I); Thermal spectra of GFP and SNCA (H) or DJ17-GFP and DJ17-SNCA (I). Negative peaks in the thermal spectra indicate high melting temperatures (Tm) for GFP and DJ17-GFP, whereas the absence of peaks in SNCA and DJ17-SNCA suggests they are intrinsically disordered proteins. (J) Quantitative analysis of (G), the co-localization of chimeric proteins with TOMM20 was calculated as a Pearson correlation coefficient in individual cells. (K) Uncoupler treatment inhibited the mitochondrial localization of DJ17-SNCA. In (B), (E), (G), and (K), representative images of two independent experiments are shown. The left images show localization of the specific chimeric or mutant proteins alone, whereas images to the right show merged images for the chimeric or mutant proteins (green) and TOMM20 (red). Asterisk in (C), (F), or (J) indicates statistically significant differences from control. Asterisk indicates $P < 0.01$ in one way ANOVA, N.S., not significant as $P > 0.01$.

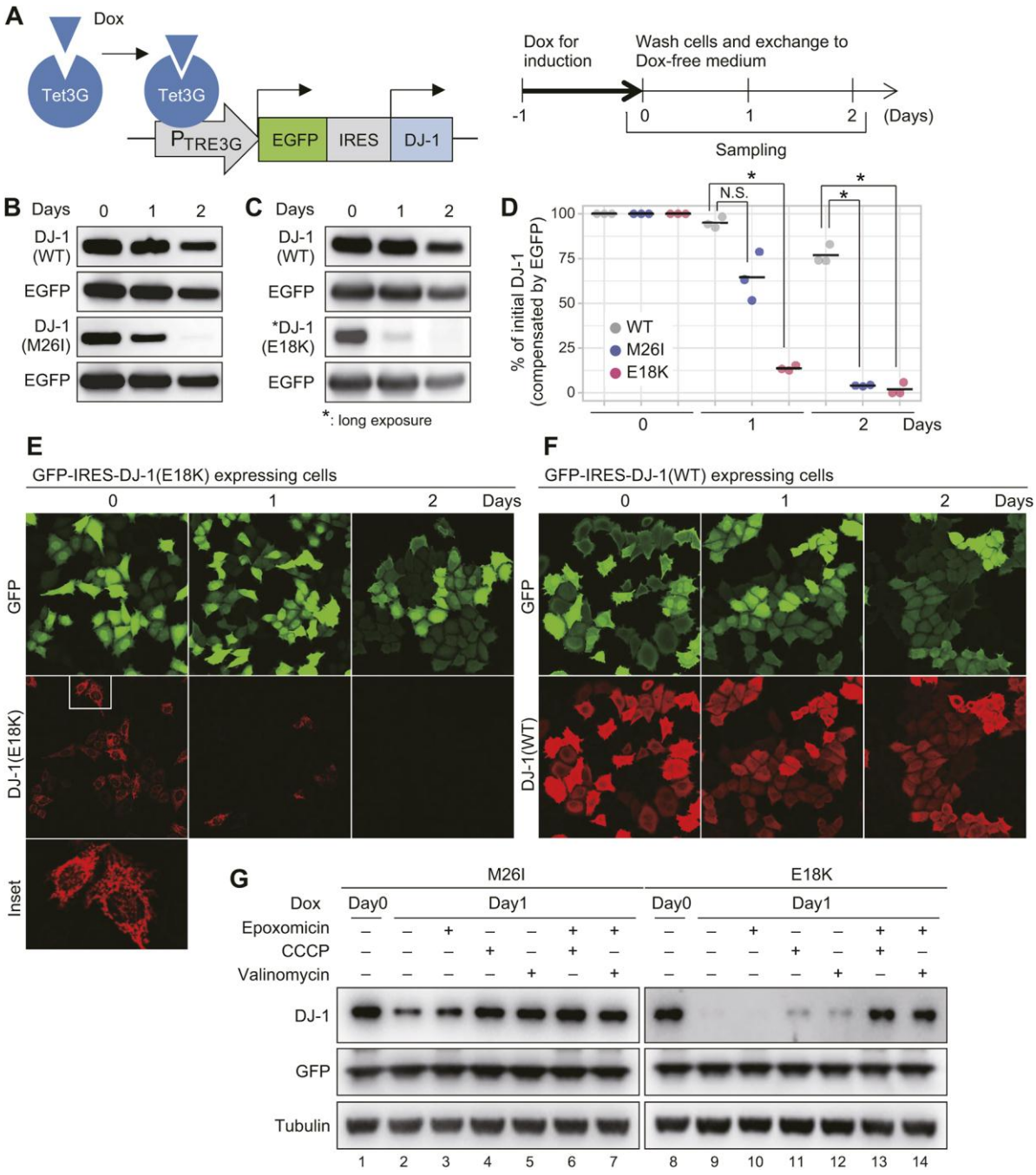

Fig. 7 –Mitochondrial import leads to DJ-1 degradation in mitochondria.

(A) Scheme for the Dox inducible system. (B) and (C): Changes in the amount of the DJ-1 mutant proteins in *DJ-1* knockout HeLa cells. Immunoblotting data for M26I (B) and E18K (C) with WT and EGFP controls are shown. Data are representative of three independent experiments. (D) Degree of protein degradation for the WT, M26I, and E18K mutants in relation to the internal EGFP control. Individual data points of three independent experiments are shown. Asterisks

indicate statistical differences between WT ($P < 0.01$). N.S., not significant as $P > 0.01$. In (E) and (F), images depict immunocytochemistry profile of cells expressing GFP-IRES-DJ-1. When E18K was co-expressed with GFP, cells positive for both GFP and mitochondrial E18K rapidly disappeared within 1 day (E). In contrast, the double positive cells persisted when wild-type DJ-1 was co-expressed with GFP (F). Reproducibility of (E) and (F) were confirmed by independent experiments. (G) Inhibition of both mitochondrial import and proteasome activity is essential for stabilization of the DJ-1 E18K mutant. Immunoblots are representative of two independent experiments.

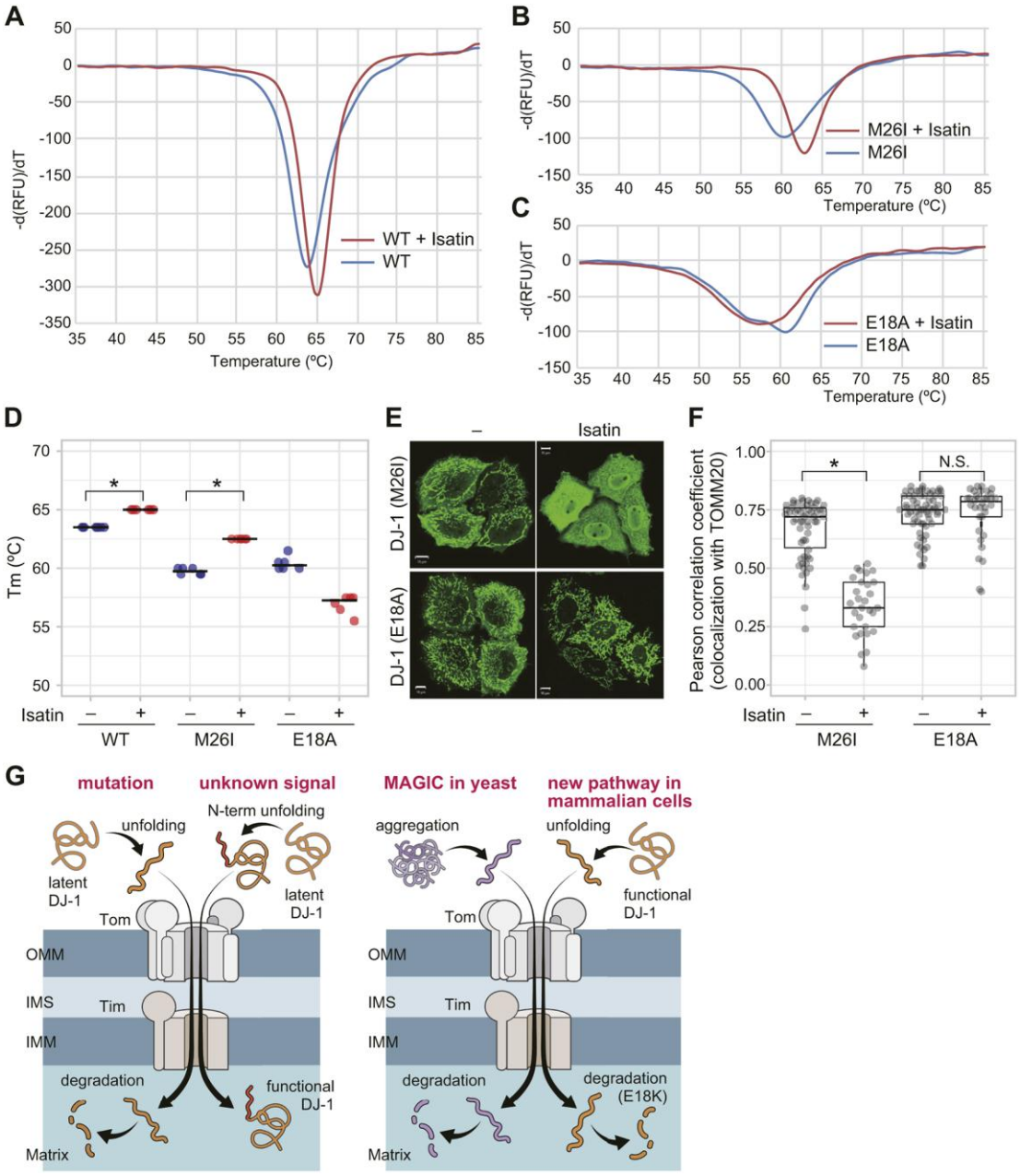

Fig. 8 –DJ-1 stabilization reverses mitochondrial localization of DJ-1 mutants.

(A) to (C): Representative thermal shift spectra for WT DJ-1 (A), M26I (B), or E18A (C) mutant in the presence of isatin. Isatin stabilizes and increases the melting temperature (Tm) of the M26I mutant but does not stabilize the E18A mutant. (D) Quantified data of the thermal shift assay are shown. Individual data points of three independent experiments are shown. Asterisks indicates statistically significant increase from untreated control ($P < 0.01$ in one way ANOVA). (E) The

subcellular localization of E18A and M26I mutants in the absence or presence of isatin when expressed in *DJ-1* knockout HeLa cells. Representative images of two independent experiments are shown. (F) The co-localization of DJ-1 M26I or E18A mutants with TOMM20 following isatin treatment was calculated as a Pearson correlation coefficient in individual cells. Asterisk indicates statistical difference between untreated control ($P < 0.01$ in one way ANOVA). N.S., not significant as $P > 0.01$. Isatin stabilization of the DJ-1 M26I mutant restores its cytoplasmic localization, whereas the isatin-insensitive E18A mutant remains localized in mitochondria. (G) Two possible schematic models for DJ-1 translocation into mitochondria. Left panel; restricted unfolding by unknown signal and subsequent mitochondrial translocation is essential for the genuine function of DJ-1, and that the mitochondria-localized DJ-1 mutants reflect this phenomenon. Right panel; mitochondrial localization of DJ-1 reflects an undetermined mitochondria-based quality control system for cytoplasmic proteins like “MAGIC” in yeast cells. See text for details.

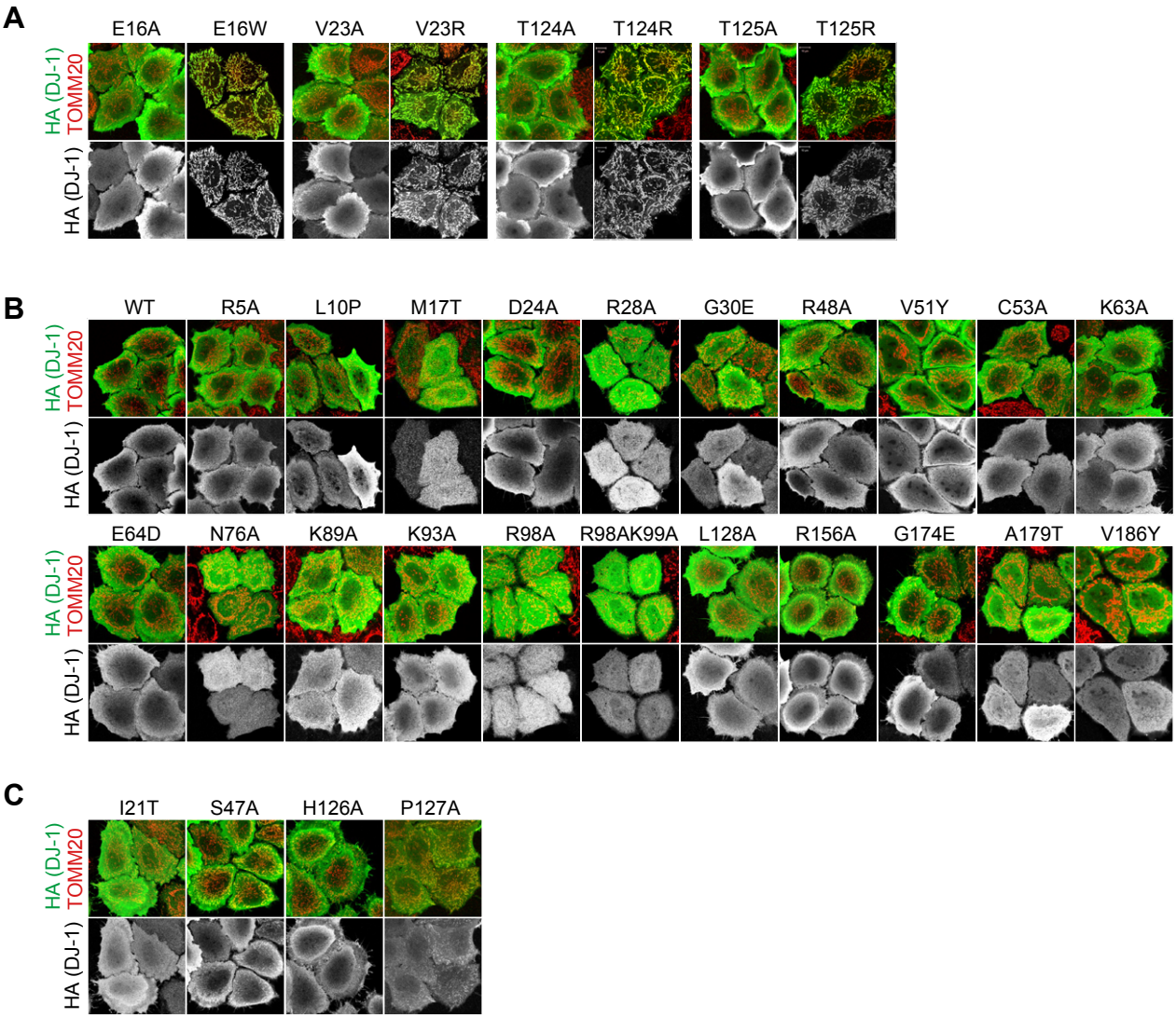

Fig. S1. (A) Representative images depicting the cytosolic localization of DJ-1 E16A, V23A, T124A, and T125A mutants with the corresponding mitochondrial localization of DJ-1 E16W, V23R, T124R, and T125R mutants. (B) Immunostaining images of DJ-1 mutants categorized as "cytosolic localization" in the quantitative analysis shown in Fig. 1D. (C) Immunostaining images of DJ-1 mutants categorized as "variable or mixed localization" in the quantitative analysis shown in Fig. 1D. In (A), (B), and (C), the top panels show localization of the DJ-1 constructs alone, and the bottom panels show merged images for the DJ-1 constructs (green) and the mitochondrial marker TOMM20 (red). All constructs were expressed in DJ-1 knockout cells.

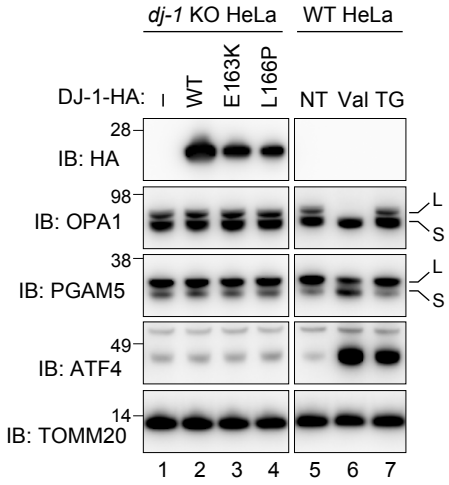

Fig. S2. No changes in the PGAM5 and OPA1 cleavage profile or the induction of ATF4 were observed following the expression of the mitochondria-localized pathogenic DJ-1 mutants E163K (lane 3) or L166P (lane 4). In contrast, when cells were treated with 10 µM Valinomycin for 3 hours (lane 6), changes to PGAM5 and Opa1 cleavage and ATF4 induction were observed. NT, cells were treated with DMSO (non-treated); Val, 10 µM valinomycin for 3 hours; TG, 300 nM thapsigargin for 3 hours.

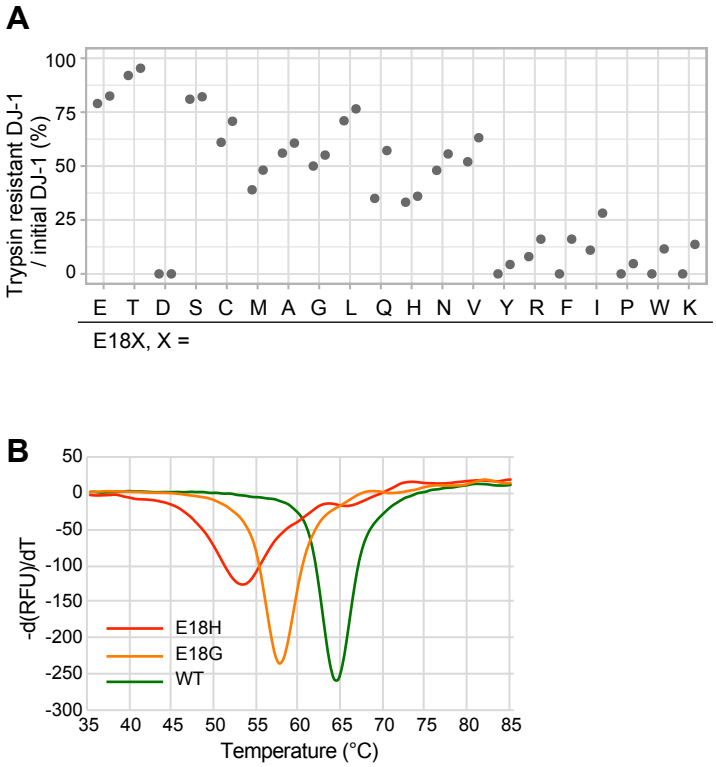

Fig. S3. (A) Recombinant C-terminal 6xHis-tagged E18X mutants were incubated with trypsin for 22 h, and the degree of trypsin sensitivity was quantified in two biological replicates. (B) Representative thermal spectra of the C-terminal 6xHis-tagged WT, E18G, and E18H DJ-1 proteins.

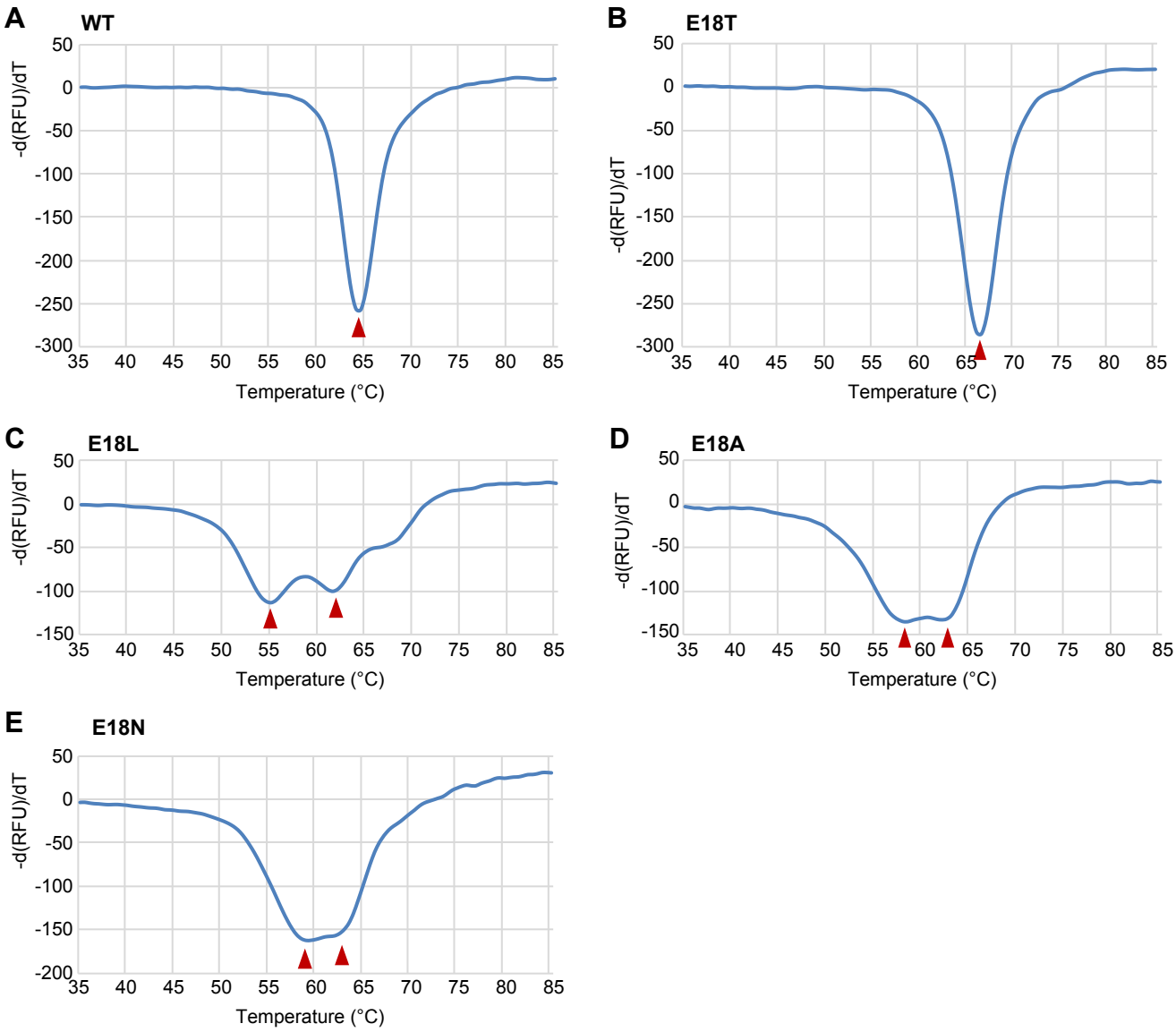

Fig. S4. Representative double-peak thermal spectra for the E18L/A/N mutants. Like WT (A), most spectra for the E18X mutants presented as a single peak for the E18T mutant (B). However, spectra for the E18L (C), E18A (D), and E18N (E) mutants had two peaks, suggesting unfolding transitions that are bimodal.

Table S1.

REAGENT or RESOURCE	SOURCE	IDENTIFIER
Antibodies		
Mouse monoclonal anti-HA (TANA2)	MBL	Cat. # M180-3, RRID:AB_10951811
Rabbit polyclonal anti-TOMM20 (FL-145)	Santa Cruz Biotechnologies	Cat. # sc-11415, RRID:AB_2207533
Rabbit polyclonal anti-TOMM20 (11802-1-AP)	Proteintech	Cat# 11802-1-AP, RRID:AB_2207530
Mouse monoclonal anti-DJ-1 (3E8)	MBL	Cat# M043-3S, RRID:AB_592469
Mouse monoclonal anti-Actin (C4)	Merck Millipore	Cat. # MAB1501R, RRID:AB_2223041
Mouse monoclonal anti-DDDDK (FLA-1)	MBL	Cat. # M185-3L, RRID:AB_11123930
Rabbit polyclonal anti-GFP (ab6556)	Abcam	Cat# ab6556, RRID:AB_305564
Rabbit polyclonal anti-PGAM5 (ab126534)	Abcam	Cat# ab126534, RRID:AB_11127076
Rabbit anti-ATF4	Cell Signaling Technology	Cat# 11815, RRID:AB_2616025
Rat monoclonal anti-Tubulin (YL1/2)	Abcam	Cat# ab6160, RRID:AB_305328
Mouse monoclonal anti-TIMM23	BD Biosciences	Cat# 611223, RRID:AB_398755
Mouse monoclonal anti-OPA1	BD Biosciences	Cat# 612606, RRID:AB_399888
Goat polyclonal anti-HSP60 (N-20)	Santa Cruz Biotechnologies	Cat. # sc-1052, RRID:AB_631683
Goat anti-Rabbit IgG Alexa Fluor 488 conjugated	Thermo Fisher Scientific	Cat# A-11034, RRID:AB_2576217
Goat anti-Rabbit IgG Alexa Fluor 568 conjugated	Thermo Fisher Scientific	Cat# A-11036, RRID:AB_10563566
Goat anti-Mouse IgG Alexa Fluor 488 conjugated	Thermo Fisher Scientific	Cat# A-11029, RRID:AB_2534088
Goat anti-Mouse IgG Alexa Fluor 568 conjugated	Thermo Fisher Scientific	Cat# A-11031, RRID:AB_144696
Goat anti-Mouse IgG Alexa Fluor 647 conjugated	Thermo Fisher Scientific	Cat# A-21236, RRID:AB_2535805
Donkey anti-Goat IgG Alexa Fluor 488 conjugated	Abcam	Cat# ab150129, RRID:AB_2687506

Donkey anti-Rabbit IgG Alexa Fluor 568 conjugated	Abcam	Cat# ab175470, RRID:AB_2783823
Goat Anti-Rabbit IgG horseradish peroxidase-linked	Jackson Immuno Research	Cat# 111-035-144, RRID:AB_2307391
Goat Anti-Mouse IgG horseradish peroxidase-linked	Jackson Immuno Research	Cat# 115-035-003, RRID:AB_10015289